Biology Direct

RESEARCH

Open Access

STAU1-mediated *CNBP* mRNA degradation by LINC00665 alters stem cell characteristics in ovarian cancer

Xiaofang Liu[1†], Yang Chen[2†], Ying Li[3†], Jinling Bai[3], Zhi Zeng[3], Min Wang[3], Yaodong Dong[4*] and Yingying Zhou[3*]

Abstract

Background To investigate the role of lncRNA LINC00665 in modulating ovarian cancer stemness and its influence on treatment resistance and cancer development.

Methods We isolated ovarian cancer stem cells (OCSCs) from the COC1 cell line using a combination of chemotherapeutic agents and growth factors, and verified their stemness through western blotting and immunofluorescence for stem cell markers. Employing bioinformatics, we identified lncRNAs associated with ovarian cancer, with a focus on LINC00665 and its interaction with the *CNBP* mRNA. In situ hybridization, immunohistochemistry, and qPCR were utilized to examine their expression and localization, alongside functional assays to determine the effects of LINC00665 on CNBP.

Results LINC00665 employs its Alu elements to interact with the 3'-UTR of *CNBP* mRNA, targeting it for degradation. This molecular crosstalk enhances stemness by promoting the STAU1-mediated decay of *CNBP* mRNA, thereby modulating the Wnt and Notch signaling cascades that are pivotal for maintaining CSC characteristics and driving tumor progression. These mechanistic insights were corroborated by a series of in vitro assays and validated in vivo using tumor xenograft models. Furthermore, we established a positive correlation between elevated CNBP levels and increased disease-free survival in patients with ovarian cancer, underscoring the prognostic value of CNBP in this context.

Conclusions lncRNA LINC00665 enhances stemness in ovarian cancer by mediating the degradation of *CNBP* mRNA, thereby identifying LINC00665 as a potential therapeutic target to counteract drug resistance and tumor recurrence associated with CSCs.

Keywords Ovarian cancer, Cancer stem cells, LINC00665, CNBP, Stemness regulation, mRNA decay, Long non-coding RNA

†Xiaofang Liu, Yang Chen and Ying Li contributed equally to this work.

*Correspondence:
Yaodong Dong
dydlxf_1218@163.com
Yingying Zhou
zyy03300821@163.com
[1]Department of Anus and Intestine Surgery, The First Affiliated Hospital of China Medical University, Shenyang, Liaoning, People's Republic of China
[2]Department of General Surgery, The First Affiliated Hospital of Liaoning University of Traditional Chinese Medicine, Shenyang, Liaoning, People's Republic of China
[3]Department of Obstetrics and Gynecology, Shengjing Hospital of China Medical University, No. 36, Sanhao Street, Shenyang, Liaoning 110004, People's Republic of China
[4]Department of Otolaryngology Head and Neck Surgery, Shengjing Hospital of China Medical University, No. 36, Sanhao Street, Shenyang, Liaoning 110004, People's Republic of China

Background

Cancer stem cells (CSCs) harbor the distinctive capacity for self-renewal, establishing themselves as a specialized subset that contributes to the complexity and malignancy of various solid tumors [1, 2]. These cells are adept at multidrug resistance [3], evading immune surveillance, and facilitating invasion and metastasis [4–7]. In specific microenvironments, CSCs can differentiate into diverse cell types, including cancerous cells, which are implicated in cancer recurrence and metastasis [2, 8, 9]. Moreover, cancer cells can dedifferentiate back into a CSC phenotype [10], thereby escaping the effects of chemotherapeutic drugs that target rapidly dividing cells. Investigating the stemness dynamics within ovarian cancer cells is therefore of critical importance, as it sheds light on the progression, recurrence, metastasis, and drug response of ovarian cancer, emphasizing the significance of CSCs as targets for therapeutic strategies.

Alu elements are short, repetitive sequences widely dispersed throughout the human genome [11]. They are a type of transposable element that can affect gene expression and genome stability [11]. Alu sequences have been implicated in various diseases, including cancer, due to their ability to mediate genomic rearrangements and influence gene regulation [12]. Recent studies have highlighted the role of Alu elements in RNA-RNA interactions, contributing to the regulation of mRNA stability and translation [12]. In the context of long non-coding RNAs (lncRNAs), Alu sequences within lncRNAs can facilitate the formation of RNA duplexes with complementary Alu elements in target mRNAs, thereby modulating their stability and expression [13]. However, the specific mechanisms by which lncRNAs regulate target gene expression through the formation of RNA duplexes with complementary Alu elements in target mRNAs, particularly in the context of ovarian cancer progression, remain largely unclear.

Staufen1 (STAU1) is a double-stranded RNA-binding protein that plays a significant role in mRNA localization, stability, and decay [14]. It is involved in a process known as Staufen-mediated mRNA decay (SMD), where STAU1 binds to specific mRNA 3'-untranslated regions (3'-UTRs), leading to mRNA degradation [14]. The interaction between STAU1 and Alu elements within mRNAs has been demonstrated to regulate the stability of various transcripts, thereby influencing gene expression [14]. This action effectively regulates the mRNA's abundance and its post-transcriptional control [15, 16]. The involvement of lncRNA in mRNA decay represents a significant mechanism that has been validated across various tumor entities [14]. LncRNAs can recruit STAU1 to target mRNAs through Alu-mediated RNA duplex formation, promoting their degradation via SMD and influencing cancer progression [17, 18]. Nonetheless, the precise mechanisms by which lncRNA-mediated mRNA decay via the SMD pathway modulates the malignant features in ovarian cancer cells remain to be fully delineated.

Cellular Nucleic Acid Binding Protein (CNBP) is a highly conserved nucleic acid-binding protein that possesses seven zinc finger motifs of the CCHC type and a region abundant in arginine and glycine (RG/RGG) [19]. It is capable of binding to nucleic acids and plays a role in the regulation of various disorders, including neuromuscular degeneration, inflammation, autoimmune conditions, and cancers [19]. In the context of cancer, CNBP has been shown to influence tumor growth and metastasis by regulating the stability and translation of specific mRNAs [20]. Currently, little is known about the role of CNBP in ovarian cancer.

In previous research, lncRNA LINC00665 was identified to show increased expression in ovarian cancer tissues, as determined by lncRNA expression profiling microarrays and bioinformatics analysis [21]. In this study, we investigate the role of LINC00665 in ovarian cancer progression, focusing on its interaction with Alu sequences, CNBP, and STAU1. We hypothesize that LINC00665 forms duplex structures with the 3'-UTRs of target mRNAs via Alu elements, facilitating STAU1-mediated *CNBP* mRNA decay and thus promoting ovarian cancer stem cell-related phenotypes. Building on this discovery, our current study reveals that LINC00665 affects the shift towards stemness in ovarian cancer cells by controlling *CNBP* mRNA stability via the SMD pathway and by altering β-catenin levels in the nucleus through the Wnt signaling pathway. These findings suggest that targeting LINC00665 could be a new approach to modulate stemness in ovarian cancer cells, offering a potential avenue for therapeutic intervention in the treatment of cancer progression and chemoresistance.

Methods

Collection of patient samples

We acquired 40 serous ovarian cancer specimens, fixed in formalin and embedded in paraffin, from individuals admitted to Shengjing Hospital of China Medical University within the timeframe of 2012 to 2017. These patients underwent conventional surgical or debulking procedures tailored to the stage of their cancer, with none having been subjected to chemotherapy or radiotherapy prior to surgery. Consent was duly obtained from all participants, and the protocol for collecting and handling patient data received approval from the Ethics Committee of China Medical University [No. 2019PS286K(X1)].

Cultivation of cells and pharmacological evaluation

The human serous epithelial ovarian carcinoma cell lines COC1 and SKOV3 were acquired from the China Center for Type Culture Collection. These cells were

incubated at 37 °C in a 5% CO_2 atmosphere. The culture was sustained in RPMI-1640 medium (31800-014, Gibco, Bristol, RI, USA), enriched with 10% fetal bovine serum (SH30084.03, Hyclone, Logan UT, USA), and the medium was refreshed after 24 h of incubation. This process was repeated until the cells reached 80% confluence. After exposure to cisplatin (40 μmol/l) and paclitaxel (10 μmol/l) [22], the cells were incubated for an additional 5 days [23]. Thereafter, the cells were propagated in conditions conducive to stem cell growth: RPMI-1640 medium (31800-014, Gibco), supplemented with recombinant human insulin (5 μg/ml) (11061-68-0, Solarbio, Beijing, China), EGF (10 ng/ml) (10,605-HNAE, Sino Biological, Beijing, China), bFGF (10 ng/ml) (10,014-HNAE, Sino Biological, China), and LIF (12 ng/ml) (RPA085Hu01, Cloud-Clone Corp., Katy, TX, USA). The medium was replaced bi-daily. After 6 days, cells were harvested for subsequent analysis of gene and protein expression.

Assay for sphere formation

To separate the spherical cell clusters, the cultures were treated with 0.25% trypsin–EDTA for 1–2 min at 37 °C. Subsequently, 100 cells were seeded per well into 96-well plates containing 200 μl of growth medium, and an additional 25 μl of the medium was supplemented to each well every two days. The count of dissociated spherical cells in each well was tallied following a 7-day incubation period.

Flow cytometry analysis

Separated cells underwent centrifugation at 1000 rpm for 5 min and were subsequently retrieved. The cells underwent a dual wash with phosphate-buffered saline (PBS; P10033, Doublehelix, Shanghai, China) and were gathered post-centrifugation at 1000 rpm for 5 min. 1×10^6 cells were suspended in 100 μl of PBS containing anti-CD133 (12-1339-41, APC, eBioscience, San Diego, CA, USA), anti-CD117 (11-1178-41, APC, eBioscience, USA), and isotype control antibodies (non-specific mouse IgG for CD133 and CD117, 70-CMG105-10, and 70-CMG104-10, MultiSciences, Hangzhou, China). The proportions of $CD133^+$ and $CD117^+$ cells were ascertained through flow cytometry following a period of incubation in darkness.

Western blotting

Proteins were isolated from COC1, SKOV3, and spheroid cell populations. The protein concentrations were quantified, and aliquots were prepared by mixing with 5× loading buffer and PBS to achieve a final concentration of 40 μg of protein in a 20 μl volume. Proteins were then subjected to SDS-polyacrylamide gel electrophoresis (SDS-PAGE) at 80 V for 2.5 h, followed by transfer onto a polyvinylidene fluoride membrane (PVDF; IPVH00010, Millipore Sigma, Burlington, MA, USA). The membranes were then blocked with non-fat dry milk and incubated with primary antibodies at 4 °C overnight, followed by incubation with the corresponding secondary antibodies at 37 °C for 45 min. The protein bands were visualized using enhanced chemiluminescence (ECL) Western blot detection reagents (Pierce, Thermo Fisher Scientific, Waltham, MA, USA) and captured with a Gel-Pro-Analyzer (WD-9413B; Beijing Liuyi, Beijing, China). β-actin (WL01845; Wanleibio, Shenyang, China) and histone H3 served as internal controls for normalization. The antibodies utilized for the immunoblotting are detailed in Table 1.

Quantitative PCR (qPCR)

RNA was isolated utilizing an RNA isolation kit (RP1201; BioTeke, Beijing, China), and its purity and concentration were assessed. 1 μg of the isolated RNA was incorporated into a 19 μl mix for reverse transcription using the PrimeScript™ RT reagent kit with gDNA Eraser

Table 1 Antibodies used in Western blotting analysis

Rabbit anti-human OCT4 antibody	1:500	Abcam, ab18976, Cambridge, UK	4 °C overnight
Rabbit anti-human SOX2 antibody	1:500	Abcam, ab97959	4 °C overnight
Rabbit anti-human NANOG antibody	1:500	Abcam, ab80892	4 °C overnight
Rabbit anti-human ALDH1 antibody	1:500	Abclonal, A0157, Hubei, China	4 °C overnight
Rabbit anti-human LGR5 antibody	1:500	Abclonal, A12327	4 °C overnight
CNBP antibody	1:400	Abclonal, A15110	4 °C overnight
Ki-67 antibody	1:500	Wanleibio, WL01384a	4 °C overnight
STAU1 antibody	1:500	Proteintech, 4225-1-AP, Rosemont, IL, USA	4 °C overnight
E-cadherin antibody	1:500	Wanleibio, WL01482	4 °C overnight
β-catenin antibody	1:500	Wanleibio, WL0962a	4 °C overnight
MDR1 antibody	1:500	Wanleibio, WL02395	4 °C overnight
β-actin antibody	1:1000	Wanleibio, WL01845	4 °C overnight
Histone H3 antibody	1:1000	Wanleibio, WL0984a	4 °C overnight
Goat anti-rabbit secondary antibody	1:5000	Abcam, ab7090	37 °C 45 min
Goat anti-rabbit secondary antibody	1:5000	Wanleibio, WLA023	37 °C 45 min

Table 2 Sequences of primers for qPCR assay

Name	Sequence	Primer length	Tm	Product length
Linc00665 F	GGTGCAAAGTGGGAAGTGTG	20	58.4	191
Linc00665 R	AGTCCGGTGGACGGATGAGAA	21	63.9	
snRNA F	CTTCAAGACTCTCTTCGTGG	20	52.0	196
snRNA R	GCCATCTGCGTGTTTGTAAG	20	56.6	
TDGF1 F	ATTTGCTCGTCCATCTCG	18	53.6	139
TDGF1 R	GGTTCTGTTTAGCTCCTTACTG	22	53.5	
β-actin F	GGCACCCAGCACAATGAA	18	57.7	137
β-actin R	CGGACTCGTCATACTCCTGCT	21	59.3	
CNBP F	TTCCAGTTTGTTTCCTCGTC	20	55	186
CNBP R	GCCACAGTTGTAGCAGCAT	19	53.9	
STAU1 F	ATCCGATTAGCCGACTGG	18	55.5	246
STAU1 R	ACTTGAGTGCGGGTTTGG	18	56.2	

Table 3 Antibodies used in immunofluorescence staining

Rabbit monoclonal antibody Lgr5	1:100	Novus Biologicals, MAB8078-SP, Centennial, CO, USA	4 °C overnight
Rabbit polyclonal antibody ALDH1	1:300	Wanleibio, WL02762	4 °C overnight
Rabbit monoclonal antibody SOX2	1:100	Abclonal, A0561	4 °C overnight
Rabbit monoclonal antibody OCT4	1:100	Affinity Biologicals, AF0226, Shanghai, China	4 °C overnight
Rabbit monoclonal antibody Nanog	1:100	Affinity, AF5388	4 °C overnight
FITC-conjugated goat anti-rabbit IgG	1:100	Abcam, ab6717	Room temperature, 1 h
Cy3-conjugated goat anti-mouse IgG	1:200	Invitrogen, A-21,424	Room temperature, 1 h

(Perfect Real Time) (RR037Q; Takara, Beijing, China). The expression levels of genes were quantified employing SYBR Green I nucleic acid gel stain (SY1020; Solarbio) on the Exicycler 96 Real-Time Quantitative Thermal Block (Bioneer, Daejeon, Korea). The sequences of the primers utilized are listed in Table 2. The thermal cycling conditions were set as follows: initial denaturation at 94 °C for 10 min, followed by 40 cycles of denaturation at 94 °C for 10 s, annealing at 60 °C for 20 s, and extension at 72 °C for 30 s, with a final extension at 72 °C for 2 min and 30 s, and a terminal hold at 40 °C for 5 min and 30 s. The melting curve analysis ramped from 60 to 94 °C, increasing by 1.0 °C every second, and concluded with a cooling step at 25 °C for 1 min. β-actin served as the endogenous reference gene for data normalization.

Immunocytochemistry

Cells were seeded onto 8-well chamber slides and cultured for 24–48 h. The slides were then fixed, rinsed, and blocked with 1% bovine serum albumin in a tris-buffered saline with Tween 20 (TBST) solution, followed by an overnight incubation at 4 °C with the designated primary antibody. Afterward, the slides were washed thrice with TBST for 10 min at 25 °C and subsequently incubated with the appropriate secondary antibody for 1 h at ambient temperature. Post-secondary antibody incubation, the slides were washed, stained with 0.5 mg/mL 4′,6-diamidino-2-phenylindole (DAPI) for 10 min, and then mounted using a fluorescence quenching prevention medium (S2100; Solarbio). Images were captured with a BX53 microscope (OLYMPUS, Tokyo, Japan). Omission of the primary antibody in the blocking solution served as the negative control. The primary and secondary antibodies utilized are detailed in Table 3.

Immunohistochemical analysis

Sections were dewaxed, immersed in antigen unmasking solution, and subjected to continuous heating for 10 min; the sections were then dried and treated with 3% hydrogen peroxide, followed by a 15-minute incubation at ambient temperature; normal goat serum was applied in a dropwise manner, and the tissue samples were further incubated for 15 more minutes at ambient temperature. The samples were subsequently incubated with the primary antibody (CNBP antibody at a 1:100 dilution in PBS) overnight within a humidified chamber at 4 °C. The samples were then treated with HRP-conjugated goat anti-rabbit IgG (1:500, #31,460; Thermo Fisher, USA) for 1 h at 37 °C, visualized using DAB chromogen (Thermo Fisher, USA), and counterstained with hematoxylin. Following this, the sections were dehydrated using absolute ethanol, cleared in xylene, set with neutral gum, and imaged using a 400× magnification microscope (DP73; OLYMPUS).

In situ hybridization

Tissue samples underwent staining, proteinase K treatment, denaturation, and subsequent in situ hybridization with probes for LINC00665 and CNBP (synthesized by Wanleibio, China). Probe detection was carried out using

a fluorescence in situ hybridization kit (GenePharma, Shanghai, China) as per the manufacturer's protocol, after which the tissue samples were counterstained with DAPI and examined under a fluorescence microscope.

Cellular transduction

Overexpression lentiviral vectors for LINC00665 (NR_038278.1, 1749 bp in length) and knockdown lentiviral vectors for CNBP were employed to transduce COC1 and SKOV3 cells, respectively. In addition, knockdown vectors for LINC00665 and overexpression vectors for CNBP (NM_001127192.2, CDS=540 bp) were used to transduce OCSCs, and knockdown vectors for STAU1 were used to transduce OCSCs or co-transduce COC1 cells with LV-LINC00665. Cells were harvested for analysis at the designated time points. STAU1 knockdown shRNA and control sequences were synthesized, and SKOV3 cells in the exponential growth phase were transfected with Lipofectamine 3000 to introduce the STAU1 knockdown fragments. The shSTAU1 with the most effective knockdown was selected for subsequent experiments.

Luciferase reporter assay

We identified an Alu element within LINC00665 and the 3'-UTR of *CNBP* mRNA [1485–1631 bp (5'-3')] through analysis with RepeatMasker software. The Alu elements were further analyzed using RNA_RNA_Anneal software, revealing a 132 bp complementary sequence with a free energy of -222.2 kcal/mol, suggesting a potential STAU1 binding site. We constructed the luciferase reporter vectors pmirGLO-CNBP-wtUTR with the wild-type (wt) *CNBP* mRNA 3'-UTR segment and pmirGLO-CNBP-mutUTR with mutations (mut) in the binding site. Additionally, we created an overexpression vector for LINC00665 (NR_038278.1, length=1749 bp) and co-transfected SKOV3 cells with either pmirGLO-CNBP-wtUTR or pmirGLO-CNBP-mutUTR. Luciferase activity was measured to assess the interaction.

RNA binding protein immunoprecipitation (RIP) assay

Cell lysates were prepared and combined with RIP immunoprecipitation buffer containing immunomagnetic beads, followed by incubation at 4 °C ranging from 3 h to overnight. After a brief centrifugation, the beads were immobilized using a magnetic separator, and the supernatant was discarded. The beads were then washed with RIP wash buffer. RNA was isolated from the immunoprecipitation complexes by protein digestion, and the presence of target RNA was detected through reverse transcription and quantitative PCR. To generate bar graphs from RNA immunoprecipitation (RIP) results, we extracted RNA post-RIP with a specific antibody, evaluated CNBP mRNA and LINC00665 levels via qPCR, and normalized them to β-actin. Using the $2^{-\Delta\Delta Ct}$ method, we calculated relative expression, followed by statistical analysis to determine the mean and standard deviation, typically from triplicate experiments. Finally, we used SPSS and GraphPad Prism to create bar graphs representing relative expression levels with error bars indicating standard deviation (SD).

MS2-RIP analysis

We constructed a LINC00665 expression and mutant construct that included an Alu sequence and an MS2 hairpin loop with an MS2 binding site (Supplymentary Table 2). These constructs were co-transfected into OCSCs along with GFP expression vectors (pMS2-GFP). Forty-eight hours post-transfection, we conducted a RIP assay on the cells using an anti-GFP antibody with the Magna RIP RNA binding protein immunoprecipitation kit (Millipore, Bedford, MA, USA) according to the manufacturer's protocol. We assessed *CNBP* mRNA levels in the immunoprecipitants by qPCR and STAU1 protein levels by western blot analysis. After altering STAU1 levels, we performed the RIP assay again and measured *CNBP* mRNA levels in the immunoprecipitants using qPCR.

Proliferation assay

Each group's cells were plated in 96-well plates at 3.5×10^3 cells per well, with quintuplicate wells per group. After overnight incubation, cells underwent viral transduction or co-transduction to alter the expression of specific genes. Post 48-h incubation at 37 °C and 5% CO_2, cell proliferation was evaluated using the CCK-8 assay as per the kit's instructions. In chemosensitivity assays, cells were treated with varying cisplatin concentrations (0, 10, 30, 50 μM) 48 h post-viral transduction. After an additional 48-h incubation, cell viability was determined by adding 10 μl of CCK-8 solution to each well and incubating for 2 h at 37 °C in 5% CO_2. Absorbance at 450 nm was recorded using a microplate reader.

Apoptosis and cell cycle analysis

Apoptosis assay: Cells from each group were cultured in 6-well plates at 5×10^5 cells per well and harvested at the specified time point. Cells were centrifuged and resuspended in 500 μl of binding buffer. Following the apoptosis detection kit's protocol, 5 μl of Annexin V-Light 650 was added and mixed thoroughly. Then, 10 μl of propidium iodide was added, mixed, and incubated at room temperature in the dark for 15 min before flowcytometry. Cell cycle analysis: Cells were collected, fixed with 70% ethanol at 4 °C for 2 h, centrifuged, and washed. The cells were then treated with 100 μl of RNase A at 37 °C for 30 min. Following this, 500 μl of propidium iodide was

added, and the cells were incubated at 4 °C in the dark for 30 min before being analyzed by flow cytometry.

Migration and invasion assay

Transwell inserts with a polycarbonate membrane were placed in 24-well plates and coated with a Matrigel matrix (Thermo Fisher, USA) to solidify. The lower chamber was filled with 800 µl of medium containing 10% FBS, and the upper chamber was filled with 200 µl of cell suspension (3×10^5 cells/well for COC1 and OCSC, and 2×10^4 cells/well for SKOV3 cells). For the migration assay, the same medium setup was used, and 200 µl of cell suspension (1×10^5 cells/well for COC1 and OCSC, and 5×10^3 cells/well for SKOV3 cells) was added to the upper chamber. After incubation, Transwell inserts with invaded or migrated cells were washed, fixed, stained, and rinsed at room temperature. OCSCs, COC1, and SKOV3 cells on the underside of the membrane were counted using an inverted microscope. The average number of cells from three fields of view was calculated for each sample.

Assessment of colony formation

OCSC and COC1 cells were subjected to a colony formation evaluation by seeding them in a medium supplemented with 0.8% methylcellulose at a concentration of 500 cells per plate. These plates were incubated at 37 °C in an atmosphere containing 5% CO_2 for a duration of 14 days before image capture. SKOV3 cells were similarly seeded and incubated under the same conditions. Post-incubation, the cells were treated with R2 reagent for staining and subsequently scanned to identify colonies. The rate of colony formation was calculated using the formula: (total colonies formed/initial cells seeded) × 100%.

Assessment of RNA stability

Two days after transfection, the cells were exposed to actinomycin D (10 µg/ml). The culture was continued, and at predetermined intervals (0, 0.5, 1, 2, 4, 8, and 16 h), mRNA was isolated. The abundance of *CNBP* mRNA at these time points was quantified via qPCR, and the mRNA half-life was deduced.

Ovarian cancer xenograft model

Female BALB/c athymic nude mice, aged six weeks, were acclimatized for one week in a controlled environment with a 12-h light/dark cycle, at 22±1 °C and 45–55% humidity, with free access to food and water. The xenograft model was established by subcutaneous injection of 1×10^5 OCSC (spheroids) into the mice. After a four-week period, the mice were sacrificed, and the tumors were harvested for further examination. The onset and growth of tumors were closely monitored, and tumor volumes were calculated using the formula: Tumor volume (mm^3) = (longest diameter × shortest diameter^2) × 0.5.

Chromatin immunoprecipitation (ChIP)

Primers were designed based on the predicted NFYA binding sites within the LINC00665 promoter region, as suggested by Jaspar. The effectiveness of these primers was confirmed by PCR using genomic DNA as a template. Cells were treated with formaldehyde for DNA-protein cross-linking, and the chromatin was subsequently fragmented ultrasonically. Protein Agarose, and Anti-NFYA antibody (100,575, Sino Biological, Wayne, PA, USA) was introduced to the supernatant for incubation. Following this, the immunoprecipitated complexes were isolated after further incubation with Protein Agarose beads. The complexes were then washed, and the cross-links between DNA and protein were reversed using NaCl. Finally, the DNA of interest was purified and subjected to PCR analysis to confirm the presence of the target sequences. The sequences of all primers utilized in the experiments are detailed in Table 4.

Bioinformatics analysis

To ascertain the long non-coding RNAs (lncRNAs) and protein-encoding genes, we utilized the RNA V5 platform (4*180K, Design ID: 076500; Agilent Technologies, Inc., Santa Clara, CA, USA) to scrutinize the lncRNAs and genes that were differentially expressed between OCSCs and COC1 cells. The procedures were executed in alignment with the guidelines provided by the manufacturer. The differentially expressed lncRNAs (DELs) and genes (DEGs) were pinpointed by evaluating the fold change (FC), with the cut-off for upregulated and downregulated genes set at an absolute FC value of 2.0 or greater. In the end, we selected a cohort of 325 lncRNAs that exhibited an absolute FC value of 2 or higher and arranged them in an ascending sequence based on the absolute value of the log fold change (Refer to Supplementary Table 1 for the leading 50 lncRNAs). Given that Staufen-mediated mRNA decay (SMD) is contingent upon the base pairing between the Alu sequence in the lncRNA and

Table 4 Primer sequences for PCR

Name	Sequence	Product length
LINC00665 F	AGGAAACAGCACCAAGGG	192
LINC00665 R	CGCTCAGTCAGCCTCAAA	
GAPDH F	TACTAGCGGTTTTACGGGCG	166
GAPDH R	TCGAACAGGAGGAGCAGAGAGCGA	

the Alu sequence in the 3'-UTR of the mRNA, our initial focus was to identify lncRNAs harboring an Alu sequence. Employing the RepeatMasker tool, we discovered an Alu sequence within LINC00665 (Supplementary Fig. 1). We retrieved the harmonized and standardized pan-cancer dataset from the UCSC database (PANCAN, $N=19{,}131$, $G=60{,}499$; https://xenabrowser.net/), which allowed us to extract the expression data for LINC00665 (ENSG00000232677) across various sample types. We then conducted a more refined screening of the samples, including solid tissue normal, primary solid tumor, primary tumor, normal tissue, primary blood-derived cancer from bone marrow, and primary blood-derived cancer from peripheral blood. Each expression value was transformed using a log2(x+1) conversion.

Collection of clinical information

We compiled data from 80 individuals diagnosed with epithelial ovarian cancer who underwent standard surgical intervention or tumor debulking tailored to the stage of cancer, with comprehensive clinical records and pathological paraffin-embedded specimens. This cohort consists of 40 cases collected during the initial pre-experimental stage from 2012 to 2017, and an additional 40 cases collected from January 2019 to December 2023, following the establishment of a new clinical sample bank in our department at Shengjing Hospital of China Medical University. These patients had not received any preoperative treatments. The cut-off for the follow-up period was set for December 2023. Pathological confirmation of epithelial ovarian cancer was obtained for all tissue samples, which were preserved in paraffin blocks. Clinical data of these patients have been shown in Supplementary Table 3. Additionally, a control group consisting of 15 patients with ovarian serous cystadenoma, who underwent either cyst nucleotomy or resection of the affected adnexa, was established. Informed consent was duly obtained from all participants, and the study received approval from the Ethics Committee of China Medical University [No. 2019PS286K(X1)].

Statistical evaluation

The statistical analysis was conducted using software packages SPSS 27.0 (IBM, SPSS, Chicago, IL, USA) and GraphPad Prism 9.0 (GraphPad Software Inc., Boston, MA, USA). Quantitative data were expressed as mean±standard deviation, while categorical data were presented in percentages. The comparison of mean values between two groups with similar variances was performed using either the Student's *t*-test (for two samples) or one-way analysis of variance (ANOVA). To assess significant differences, non-parametric tests such as the Unpaired Wilcoxon Rank Sum and Signed Rank Tests were employed. Survival rates were determined using the Kaplan–Meier plotter [24] and the log-rank test, while Pearson correlation analysis was utilized to examine the relationships between different groups. A *P*-value of less than 0.05 was considered to indicate statistical significance.

Results

Isolation and identification of ovarian cancer stem cells

The isolation of cancer stem cells can be achieved by sorting side population (SP) cells from ovarian cancer cell populations through the efflux of Hoechst 33,342 dye, a process that can be inhibited by verapamil treatment [25]. Alternatively, the presence of cancer stem cells can be confirmed by identifying cells expressing surface markers indicative of pluripotency, such as $CD44^+$, $CD133^+$, and $CD117^+$, using flow cytometric analysis [24–26]. In our quest to understand the factors influencing the stemness characteristics of ovarian cancer cells, we adopted a low-density cell culture technique. The COC1 ovarian cancer cell line was cultivated in a serum-deprived medium supplemented with various growth factors to promote the emergence of cells with stem-like properties. The surface markers $CD117^+$ and $CD133^+$ were utilized to identify ovarian cancer stem cell-like cells. Following treatment with chemotherapeutic agents (cisplatin and paclitaxel), COC1 cells were maintained in a medium conditioned for stem cells, which included recombinant human insulin, EGF, bFGF, and LIF. Analysis via flow cytometry of the resultant cell aggregates indicated a significantly greater frequency of $CD117^+/CD133^+$ cells compared to untreated COC1 cells ($^*P<0.05$). The presence of stem cell-associated proteins was assessed through western blotting and immunofluorescence techniques, with a comparative analysis against COC1 cells. This analysis revealed elevated levels of stemness-related proteins SOX2, OCT4, and NANOG in the treated cells. Additionally, the levels of ALDH1 and LGR5, two specific markers for ovarian cancer stem cells, were found to be enhanced (Supplementary Fig. 2). These $CD117^+/CD133^+$ cells were thus designated as ovarian cancer stem cells (OCSCs).

Bioinformatics-based prediction of protein-coding and long non-coding RNAs involved in stemness regulation in ovarian cancer cells

Dysregulated lncRNAs play a pivotal role in the stemness transition of neoplastic cells [27–30]. LncRNAs can modulate the expression of protein-coding genes either directly or indirectly [29]. Our findings indicated that in epithelial ovarian cancer, LINC00665 levels were significantly elevated in tumor samples compared to normal ovarian tissues (tumor: 5.75±0.92; normal: 4.12±0.51, $P=0.013$) (Fig. 1A, a). Kaplan–Meier survival analysis of ovarian cancer cases from the GEO, EGA, and TCGA

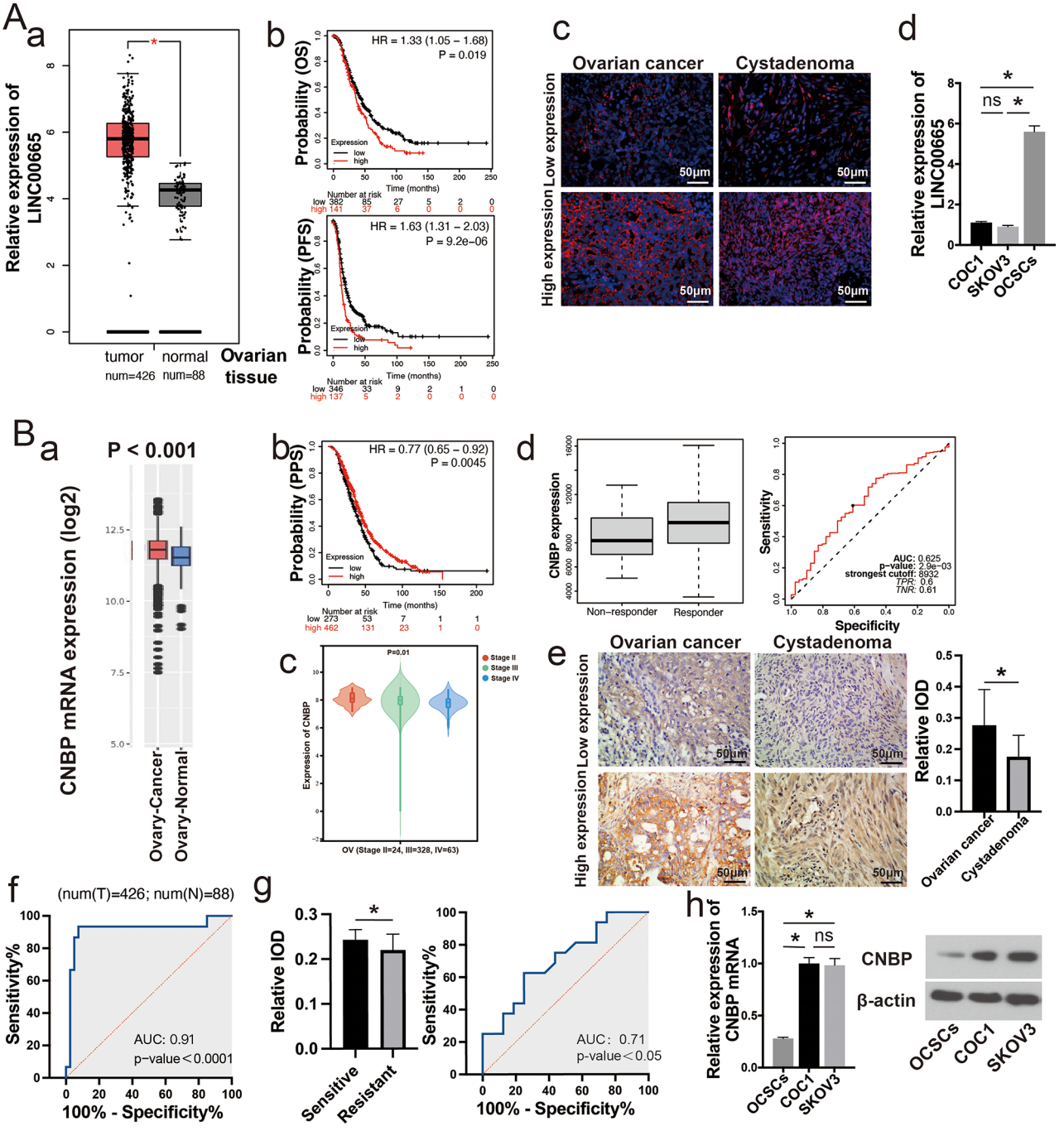

Fig. 1 Prediction and validation of RNAs associated with the regulation of stemness of ovarian cancer cells **(A) a**. Differential expression of LINC00665 in epithelial ovarian cancer versus normal tissues analyzed by TCGA TARGET GTEx. **b**. Relationship between LINC00665 and ovarian cancer prognosis analyzed by Kaplan–Meier plotter. **c**. Expression and cellular localization of LINC00665 in benign and malignant ovarian tumors detected by in situ hybridization. **d**. Differential expression of LINC00665 in OCSC and epithelial ovarian cancer cells detected by qPCR. **(B) a**. Differential expression of *CNBP* in epithelial ovarian cancer versus normal tissues analyzed by GENT2. **b**. The relationship between *CNBP* expression and ovarian cancer prognosis was analyzed by the Kaplan–Meier plotter. **c**. Differences in *CNBP* expression in samples from ovarian cancer of different clinical stages. **d**. Differences in *CNBP* expression between responders and non-responders. **e**. Expression and cellular localization of CNBP in benign and malignant ovarian tumors detected by immunohistochemical assays. **f**. The diagnostic value of ROC curve analysis of CNBP in epithelial ovarian cancer. **g**. Differential expression of CNBP protein in drug-resistant and sensitive ovarian cancer tissues (left) and the diagnostic value of ROC curve analysis of CNBP in chemotherapy resistance of ovarian cancer (right). **h**. Differences in the expression of CNBP mRNA and CNBP in OCSC and epithelial ovarian cancer cells detected by qPCR and western blotting, **P* < 0.05

databases revealed that patients with high LINC00665 expression had reduced overall survival (OS, 36.4 months vs. 45 months, HR = 1.33 [1.05–1.68], $P = 0.019$) and disease-free survival (DFS, 12.83 months vs. 18.27 months, HR = 1.63 [1.31–2.03], $P = 9.2e\text{-}06$) compared to those with low LINC00665 expression (Fig. 1A, b).

The subcellular distribution of LINC00665 was predicted using an online tool (http://www.csbio.sjtu.edu.cn/bioinf/lncLocator/ [33]), which suggested that LINC00665 transcripts are predominantly located in the cytosol and cytoplasm (Supplementary Fig. 3). In situ hybridization and qPCR confirmed that LINC00665 was mainly found in the cytoplasm of ovarian cancer tissues, whereas it was present in both the nucleus and cytoplasm of serous cystadenoma tissues (Fig. 1A, c; Supplementary Fig. 3). LINC00665 levels were higher in OCSCs compared to COC1 and SKOV3 ovarian cancer cell lines (Fig. 1A, d).

Utilizing datasets GSE80373 and GSE145374 from the GEO repository, a cohort of 1016 DEGs were identified as the differentially expressed mRNAs between OCSC and the respective control. These genes were predominantly associated with critical cellular pathways such as p53 signaling, Notch signaling, and metabolic processes, hinting at their potential role in the modulation of stemness within ovarian cancer cells (Supplementary Fig. 4). The StarBase platform [34] was employed to pinpoint mRNAs of protein-coding genes that might interact with LINC00665, and these were cross-referenced with the previously identified 1016 DEGs. This comparative approach yielded nine genes of interest: *HKR1*, *SUN1*, *TMTC4*, *IDH1*, *CNBP*, *RBM19*, *EIF4A2*, *EEF1A1*, and *PSMD9*. An Alu element within the 3'-UTR of *CNBP* mRNA was discovered through RepeatMasker analysis. Subsequent scrutiny using RNA_RNA_Anneal software [11] disclosed a 132 bp sequence within this Alu element that is complementary to the Alu sequence in LINC00665, exhibiting a significant free energy of −222.2 kcal/mol (Supplementary Fig. 5).

Using the GENT2 database, we extracted expression data for the ENSG00000169714 (*CNBP*) gene to assess its mRNA levels in ovarian cancer. The analysis showed that CNBP expression was markedly increased in ovarian cancer tissues compared to normal ovarian tissues ($P < 0.001$) (Fig. 1B, a). To determine the impact of CNBP levels on patient outcomes, survival analysis was conducted using the Kaplan–Meier plotter, incorporating data from the GEO, EGA, and TCGA databases. Patients with elevated CNBP expression exhibited a decreased overall survival (OS) (35 months vs. 45 months, HR = 1.32 [1.06–1.66], $P = 0.014$), a reduced progression-free survival (PFS) (11.53 months vs. 18 months, HR = 1.7 [1.37–2.12], $P = 1.6e\text{-}06$), but an extended post-progression survival (PPS) (42.63 months vs. 37 months, HR = 0.77 [0.65–0.92], $P = 0.0045$) (Fig. 1B, b). The CNBP expression was more pronounced in stage II and III ovarian cancers compared to stage IV ($P < 0.01$), with no significant difference between stages II and III ($P = 0.16$) (Fig. 1B, c). In grade 3 ovarian cancer patients treated with platinum and paclitaxel chemotherapy (https://www.rocplot.org/ovarian/index) [35], those who responded to chemotherapy within 6 months had higher CNBP expression than those who did not respond (Fig. 1B, d). The gene-based classification of treatment response showed potential of CNBP expression in distinguishing between responder and non-responder patients with an AUC of 0.625; $P = 0.0039$ (Fig. 1B, d). These findings underscore the significant association of CNBP with the progression and prognosis of ovarian cancer.

Immunohistochemical analysis revealed that in serous ovarian carcinoma, CNBP predominantly resided in the cytoplasm, irrespective of its expression levels, with occasional nuclear presence observed in certain cells. In contrast, in serous cystadenoma, high CNBP expression was noted within the nuclei of cells. Comparative immunohistochemical studies between epithelial ovarian cancer tissues and ovarian serous cystadenoma indicated a significantly higher expression of CNBP protein in the former (Fig. 1B, e). ROC curve analysis suggested that elevated CNBP levels could serve as a potential marker for distinguishing between epithelial ovarian tumors (AUC = 0.91, $P < 0.05$) (Fig. 1B, f). The patient cohort under study received 6–8 cycles of paclitaxel-carboplatin (TC) chemotherapy. Sixteen cases were categorized as the drug-resistant group due to recurrence within six months post-treatment (evidenced by increased CA125 and imaging) or lack of response to therapy, while another 16 cases, showing no recurrence or recurrence after six months, were deemed the sensitive group. The analysis indicated that CNBP protein expression was significantly higher in the sensitive group compared to the drug-resistant group ($P < 0.05$). Additional ROC curve analysis demonstrated that CNBP expression could effectively predict the response of epithelial ovarian tumors to chemotherapy (AUC = 0.71, $P < 0.05$) (Fig. 1B, g). In both serous ovarian cancer and serous cystadenoma, high LINC00665 expression correlated with reduced CNBP expression. Furthermore, *CNBP* mRNA levels and protein expression in OCSC were found to be lower than those in COC1 and SKOV3 cells (Fig. 1B, h). The comprehensive flow diagram of the study is depicted in Fig. 2.

Interaction between LINC00665 and *CNBP* mRNA 3'-UTR through alu elements facilitates mRNA degradation

Subsequently, we confirmed the direct interaction between the Alu sequence of LINC00665 and the Alu sequence within the 3'-UTR of *CNBP* mRNA. By employing a luciferase reporter assay in 293T cells, we observed

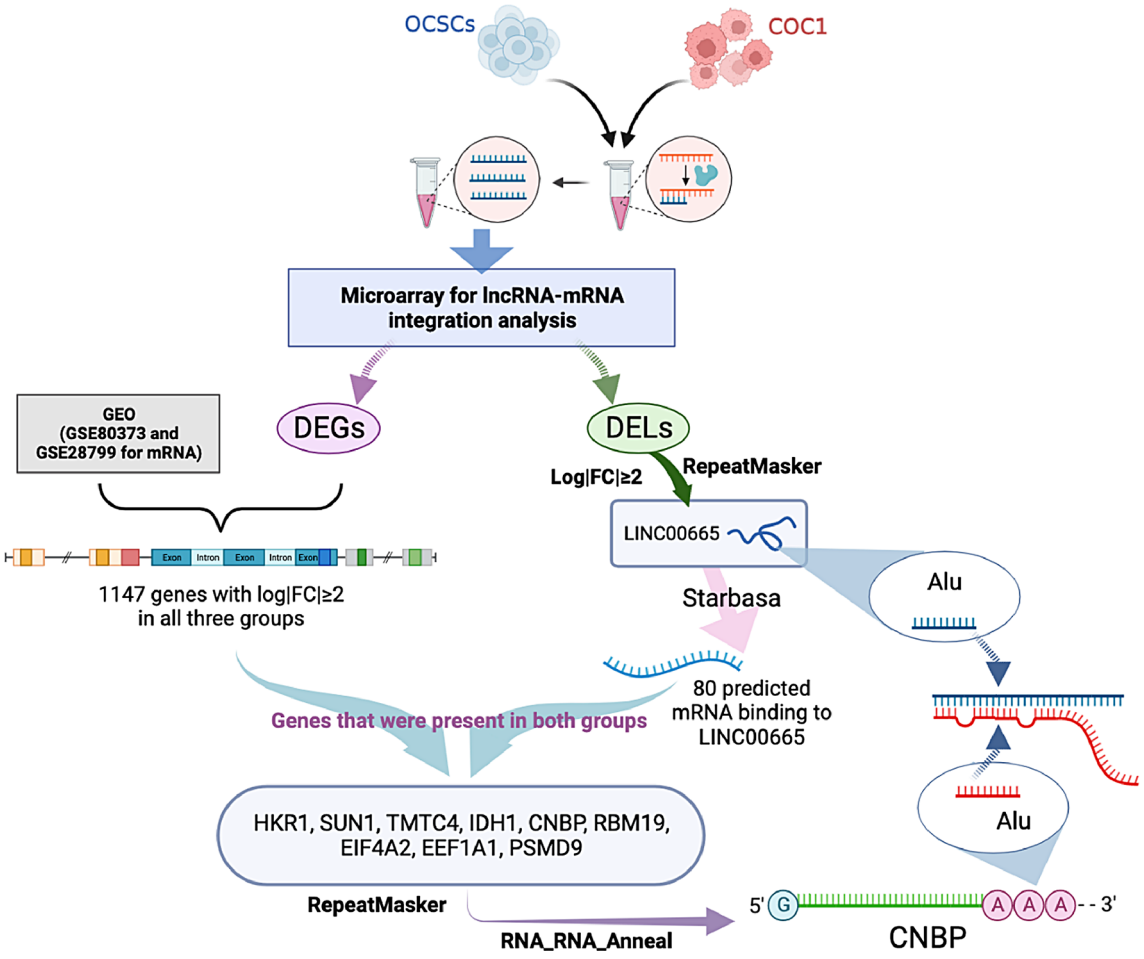

Fig. 2 Flowchart of bioinformatics analysis of LINC00665 and CNBP

that LINC00665 markedly decreased the luciferase activity of constructs containing the wild-type *CNBP* mRNA 3'-UTR Alu sequence ($P<0.05$). This suppressive effect of LINC00665 was not observed with mutant constructs (Fig. 3A).

To validate the direct association of STAU1 with both LINC00665 and the *CNBP* mRNA 3'-UTR, we used anti-STAU1 antibodies to precipitate the complex from OCSC lysates. The qPCR analysis confirmed the enrichment of both *CNBP* 3'-UTR and LINC00665 in the precipitated samples (Fig. 3B).

To demonstrate the direct interaction of LINC00665 with the *CNBP* mRNA 3'-UTR mediated by STAU1, we constructed an overexpression vector for LINC00665 with an MS2 stem-loop and co-transfected it with a GFP overexpression vector pMS2-GFP into OCSCs. Immunoprecipitation with anti-GFP antibodies and subsequent western blotting analysis showed STAU1 presence in the MS2-LINC00665-wt immune complex containing the intact LINC00665 Alu sequence. In contrast, STAU1 was absent in the complex with the mutated MS2-LINC00665-mut (Fig. 3C, a). qPCR analysis indicated a significantly higher *CNBP* mRNA level in the MS2-LINC00665-wt immune complex compared to the MS2-LINC00665-mut and the negative control (Fig. 3C, b). Upon STAU1 knockdown in the MS2-LINC00665-wt complex, qPCR revealed a reduction in *CNBP* mRNA levels, although they remained elevated compared to the MS2-LINC00665-mut and negative control (Fig. 3D). These findings suggest that the Alu element of LINC00665 is associated with the *CNBP* mRNA 3'-UTR in an STAU1-dependent manner.

To further substantiate the influence of STAU1 on CNBP, we assessed the levels of STAU1 and CNBP in OCSCs and COC1 cells through western blotting. The findings indicated that STAU1 levels were elevated in OCSCs compared to COC1 cells. In contrast, CNBP levels were found to be lower in OCSC than in COC1 cells, displaying an inverse relationship with STAU1. To delve deeper into the effects of STAU1 on CNBP regulation, we suppressed STAU1 expression in OCSCs. Subsequent evaluations revealed an increase in both mRNA and protein levels of CNBP in OCSCs with reduced STAU1 expression (Fig. 3E, a, b). However, LINC00665 levels

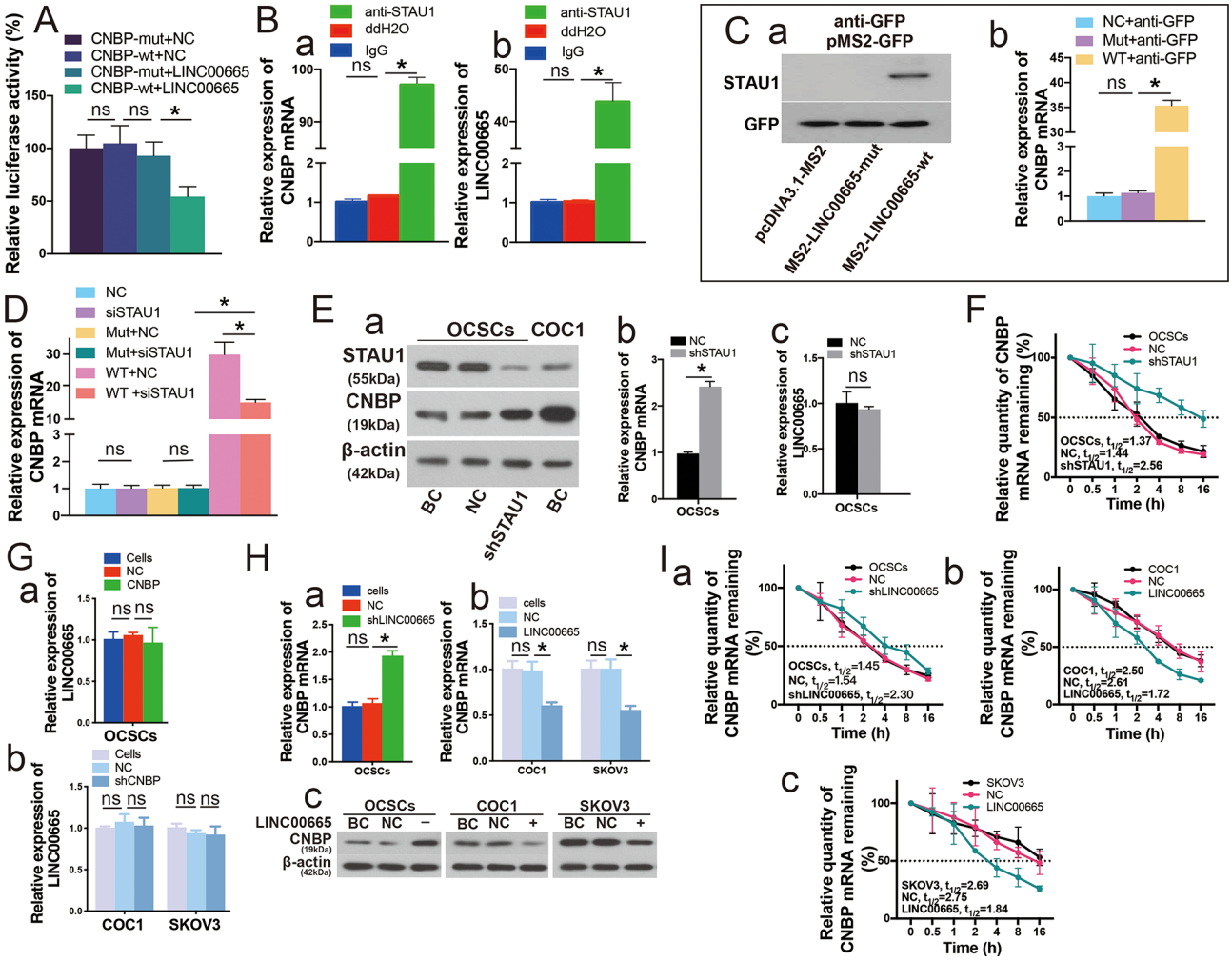

Fig. 3 LINC00665 promotes *CNBP* mRNA decay by forming duplexes with 3′-UTRs via Alu elements **(A)** Effect of LINC00665 on the fluorescent expression of reporter gene vectors containing the *CNBP* mRNA 3′-UTR Alu element in 293T cells 48 h after transfection in the luciferase reporter assay. **(B)** RNA immunoprecipitation (RIP) was performed with a STAU1-specific antibody. The RNA was extracted, and CNBP mRNA and LINC00665 levels were evaluated by qPCR. **a**. The relative expression of CNBP mRNA, **b**. The relative expression of LINC00665. **C.** MS2-RIP followed by western blotting and qPCR to detect STAU1 and *CNBP* mRNA separately associated with LINC00665. **a**. Western blot for STAU1, **b**. qPCR for *CNBP* mRNA. **D.** MS2-RIP followed by qPCR to detect *CNBP* mRNA associated with LINC00665 after inhibiting the expression of STAU1. **E.** Expression of STAU1 and CNBP in OCSC and COC1 cells, and the effect of STAU1 inhibition on the expression of CNBP and LINC00665. **a**. Western blotting results after inhibition of STAU1. **b**. *CNBP* mRNA detected by qPCR. **c**. LINC00665 detected by qPCR. **F.** The stability of *CNBP* mRNA in OCSCs treated with shSTAU1. **G.** Expression of LINC00665 in each group of cells detected by qPCR after modulating CNBP expression: **a**. CNBP overexpression in OCSCs; **b**. Suppression of CNBP expression in COC1 and SKOV3 cells. **H.** After modulating LINC00665 expression, the expression of CNBP mRNA and CNBP protein in each group of cells was detected by qPCR and western blotting, respectively: **a**. qPCR assay after inhibiting LINC00665 expression in OCSC; **b**. qPCR assay after overexpression of LINC00665 in COC1 and SKOV3; and c. Western blot results. **I.** The stability of *CNBP* mRNA in cells transfected with the indicated vectors: **a**. OCSCs treated with shLINC00665, **b**. COC1 and **c**. SKOV3 ovarian cancer cells treated with LV-LINC00665, **P* < 0.05

remained unchanged, implying that STAU1 alterations do not influence LINC00665 expression (Fig. 3E, c).

Additionally, we examined the impact of STAU1 on *CNBP* mRNA stability by employing actinomycin D to inhibit transcription. The data indicated that the downregulation of STAU1 extended the half-life of *CNBP* mRNA in OCSCs (2.56 h) compared to the control group (1.44 h) ($P<0.05$, Fig. 3F).

Altering CNBP expression did not result in changes in LINC00665 levels across all cell lines tested (Fig. 3G). Experiments modulating LINC00665 expression demonstrated that in OCSCs with reduced LINC00665, there was an increase in CNBP mRNA and protein levels, and the half-life of CNBP mRNA was extended, suggesting enhanced mRNA stability. Conversely, in COC1 and SKOV3 cells with increased LINC00665 expression, there was a decrease in CNBP mRNA and protein levels, and the half-life of CNBP mRNA was reduced, suggesting reduced mRNA stability. All observed differences were statistically significant ($P<0.05$, Fig. 3H and I).

CNBP is involved in the modulation of stemness dynamics in ovarian cancer cells

A lentiviral vector for the overexpression of CNBP was engineered and used to transduce OCSCs. At 48 h post-transduction, a comparative analysis with the control group revealed a notable reduction in the sphere formation of CNBP-overexpressing OCSCs, a significant decline in the proportion of $CD133^+/CD117^+$ cells relative to the total cell population (Fig. 4A, Supplementary Fig. 6), and a marked decrease in the proliferative potential of CNBP-overexpressing OCSCs (Fig. 4B, a).

We developed a vector to suppress CNBP expression and introduced it into COC1 and SKOV3 cells. Post-transfection at 48 h, the proliferative capacity of

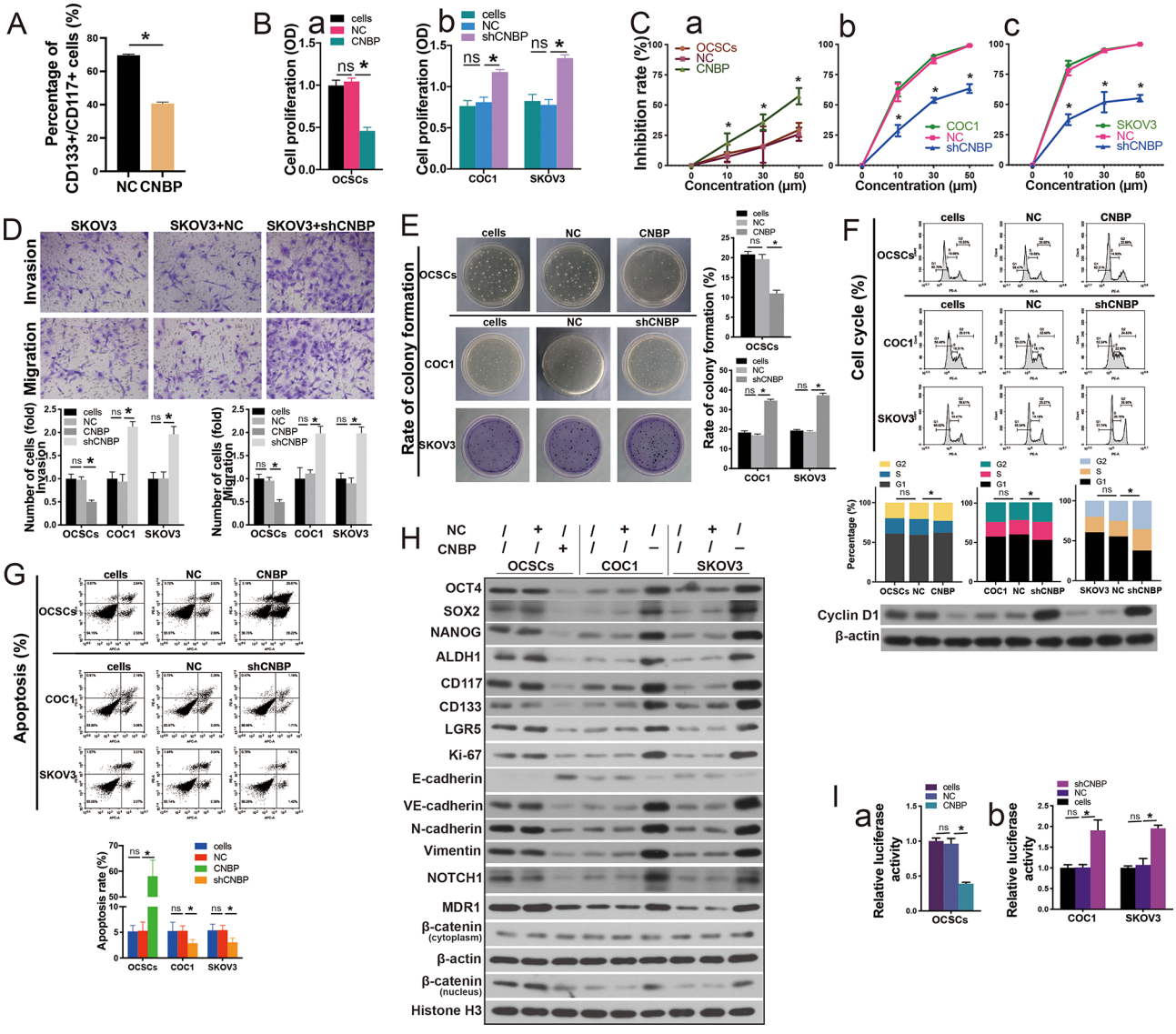

Fig. 4 CNBP regulates the stemness transition of ovarian cancer cells **(A)** Sphere formation of OCSC overexpressing CNBP, and percentage of $CD133^+/CD117^+$ cells overexpressing CNBP to total cells detected by flow cytometry. **(B)** Effects of CNBP on cell proliferation detected by using CCK-8 assay: **a**. Overexpression of CNBP in OCSCs; **b**. Inhibition of CNBP expression in COC1 and SKOV3 cells. **C.** Differences in the inhibition rate of each group of cells treated with different concentrations of cisplatin after modulating the expression of CNBP: The cells of each group were added with different concentrations of cisplatin (0, 10, 30, 50 μM) and then continued to be cultured for 48 h. The effect of different concentrations of cisplatin on the inhibition rate of each group of cells after regulating the expression of CNBP was detected by using CCK-8 assay: **a**. OCSC overexpressing CNBP; **b** and **c**. Suppression of CNBP expression in COC1 and SKOV3 cells. Detection of cell biological behaviors after modulating CNBP expression in each group of cells: overexpression of CNBP in OCSC and inhibition of CNBP expression in COC1 and SKOV3 cells. **D.** Cell migration and invasion were measured by transwell assays. **E.** Colony formation assays for each group of cells; **F.** Cell cycle percentage assays for each group of cells; **G.** Apoptotic percentage assays for each group of cells; **H.** Detection of relevant protein expression in each group of cells by western blotting. **I.** The effect of CNBP on the activity of the Wnt pathway in each group of cells was detected. The relative fluorescence activity of each group of cells was assayed after transfection with TOPFlash/FOPFlash vectors: **a**. OCSC overexpressing CNBP; **b**. COC1 and SKOV3 cells with suppressed CNBP expression, $^*P < 0.05$

these cells was significantly augmented (Fig. 4B, b). Subsequently, we treated the cells with varying cisplatin concentrations (0, 10, 30, 50 μM) and continued the incubation for an additional 48 h. The findings demonstrated that the suppressive impact of cisplatin on OCSC with elevated CNBP expression was significantly intensified in a dose-dependent manner, whereas the suppressive effect was notably reduced in COC1 and SKOV3 cells with diminished CNBP expression (Fig. 4C).

Additionally, OCSCs with increased CNBP expression exhibited reduced capabilities for invasion, metastasis, and colony formation (Fig. 4D, E). Conversely, COC1 and SKOV3 cells with downregulated CNBP expression displayed increased invasive, metastatic, and colony-forming activities (Fig. 4D, E). When compared to the control group, the overexpression of CNBP led to a reduced entry of OCSCs into the S-phase of the cell cycle and a substantial elevation in apoptotic events (Fig. 4F, G). On the other hand, the suppression of CNBP expression in COC1 and SKOV3 cells resulted in an increased transition into the S-phase, a significant reduction in apoptosis, and associated alterations in Cyclin-D1 expression (Fig. 4F, G). These observations imply that CNBP has the capacity to suppress cellular proliferation and trigger apoptosis by inducing arrest in the S-phase of the cell cycle.

In our analysis of GSE106918, the CNBP-binding mRNAs identified were subjected to KEGG pathway analysis and network construction. This analysis highlighted pathways pertinent to CSC, including those involved in Wnt, p53, Hippo, and VEGF signaling pathways, as well as those implicated in cancer, resistance to platinum-based drugs, PD-L1 expression and PD-1 checkpoint pathways, and Notch, MAPK, and HIF-1 signaling pathways, including those that regulate the pluripotency of stem cells (Supplementary Fig. 7). These pathways are linked to the preservation and transition of stemness, leading us to select proteins within these pathways for further validation in OCSCs.

Our investigation demonstrated that in OCSCs, the enhancement of CNBP levels led to a suppression of stem cell markers such as OCT4, SOX2, NANOG, LGR5, and ALDH1, as well as a reduction in the surface markers CD117 and CD133. This was accompanied by a decrease in Ki-67 expression, indicative of reduced cellular proliferation. Furthermore, the upregulation of CNBP was associated with an increase in E-cadherin levels and a decrease in VE-cadherin, N-cadherin, and Vimentin expression, aligning with the observed reduction in invasive and metastatic capabilities of OCSCs. The expression of NOTCH1 was also diminished, implying a potential inhibition of the Notch signaling pathway by CNBP overexpression. Additionally, there was a decrease in MDR1 expression, which is linked to multidrug resistance, and a reduction in nuclear β-catenin levels, although cytoplasmic β-catenin levels remained unchanged (Fig. 4H, left panel). The introduction of TOPFlash/FOPFlash vectors and subsequent dual-luciferase assays indicated a lower TOPFlash/FOPFlash fluorescence ratio in the group with CNBP overexpression, suggesting a dampening effect on Wnt pathway activity (Fig. 4I, a). Conversely, the downregulation of CNBP in COC1 and SKOV3 cells resulted in an upsurge of the aforementioned stem cell markers and proteins associated with invasiveness and drug resistance, a decrease in E-cadherin expression, and an increase in nuclear β-catenin, without impacting cytoplasmic β-catenin (Fig. 4H, middle and right panels). The fluorescence ratio was also found to be higher in these cells, indicating an activation of the Wnt pathway, likely due to the suppression of CNBP (Fig. 4I, b). Our findings suggest that enhanced CNBP levels in OCSCs suppressed stem cell markers, reduced proliferation, and inhibited invasion, potentially via modulation of the Notch and Wnt pathways.

LINC00665 fosters stemness characteristics in ovarian cancer cells through the downregulation of CNBP

Simultaneous manipulation of LINC00665 and CNBP levels was performed in our study. Initially, we observed that the suppression of LINC00665 led to a reduction in both the sphere formation capacity of OCSCs and the proportion of $CD133^+/CD117^+$ cells relative to the total cell population when compared to the control group. On the other hand, the downregulation of CNBP resulted in a resurgence of sphere-forming OCSCs and an increased ratio of $CD133^+/CD117^+$ cells (Supplementary Fig. 8). The growth rate of OCSCs with diminished LINC00665 levels was notably lower than that of the control group. This reduction in cell proliferation was reversed upon the subsequent downregulation of CNBP. Noting that LINC00665 levels in COC1 and SKOV3 cells were inferior to those in OCSCs, we proceeded to induce overexpression of LINC00665 in these cell lines. The data indicated that LINC00665 augmentation markedly promoted cell proliferation across the groups in comparison to the control. Yet, when both LINC00665 and CNBP were overexpressed in COC1 and SKOV3 cells, a significant decline in cell proliferation was recorded (Fig. 5A). Consistent with previous steps, we treated the various cell groups with escalating doses of cisplatin and monitored the outcomes. The findings demonstrated that the rate of cisplatin-induced inhibition was substantially elevated in OCSCs with LINC00665 downregulation at higher concentrations, reduced in OCSCs with concurrent suppression of LINC00665 and CNBP, diminished in COC1 and SKOV3 cells with LINC00665 upregulation, and escalated in OCSCs with upregulation of both

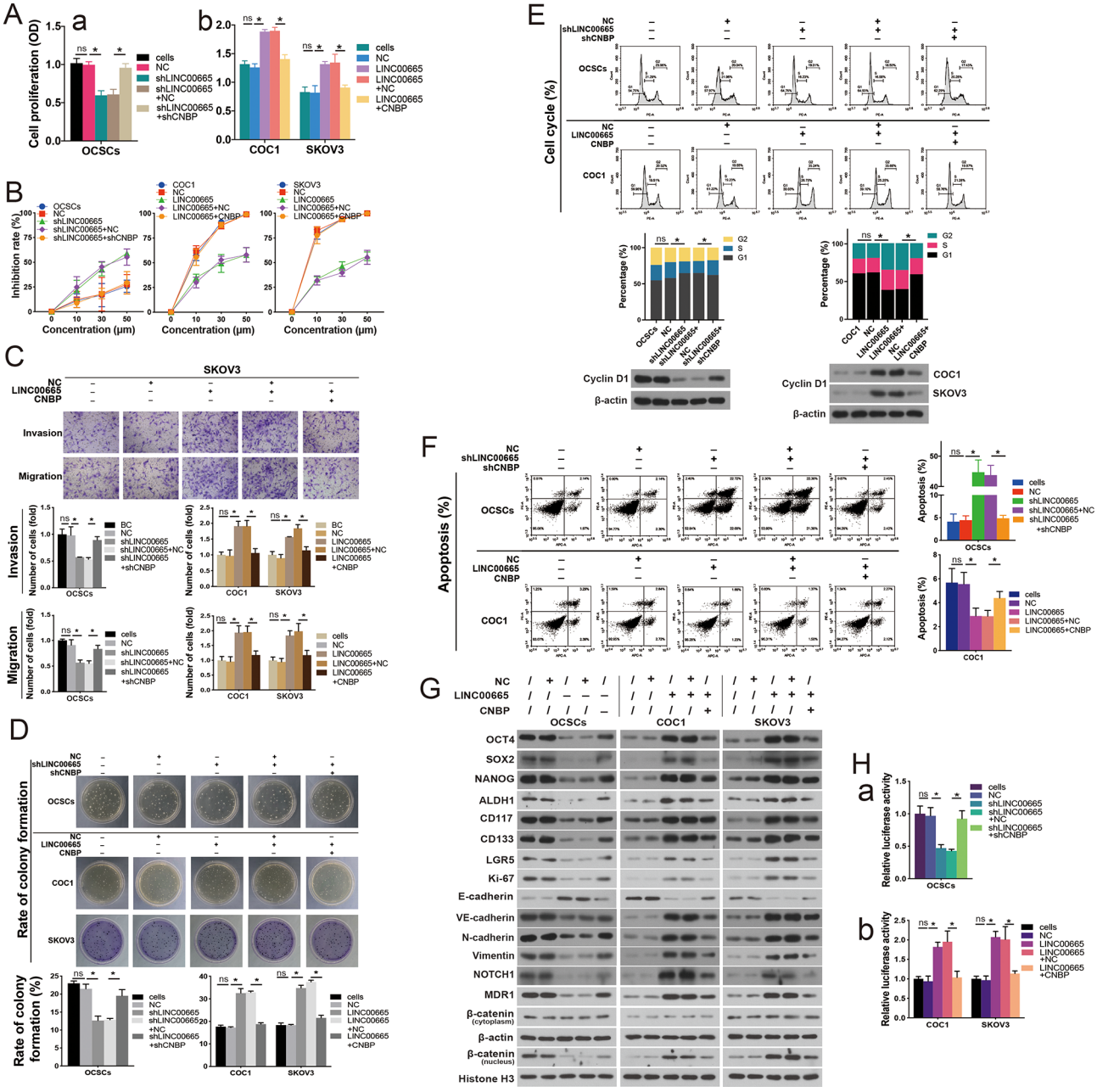

Fig. 5 LINC00665 promotes stemness transition of ovarian cancer cells by mediating CNBP expression **A.** The effects of CNBP and LINC00665 expression regulation on cell proliferation were detected using CCK-8 assays: **a**. LINC00665 and CNBP expression was modulated in OCSC; **b**. LINC00665 and CNBP expression was modulated in COC1 and SKOV3 cells. **B.** Differences in the inhibition rate of cells in each group with a modulated expression of LINC00665 and CNBP by different concentrations of cisplatin were detected: cells in each group were added with different concentrations of cisplatin (0, 10, 30, and 50 μM) and then continued to be cultured for 48 h. The inhibition rate of (**a**) OCSCs, (**b**) COC1 cells, and (**c**) SKOV3 cells with modulated expression of LINC00665 and CNBP by different concentrations of cisplatin was detected by using CCK-8 assays. The cell biological behaviors of each group of cells after modulating the expression of CNBP and LINC00665 were detected: the expression of LINC00665 and CNBP was co-repressed in OCSC and co-overexpressed in COC1 and SKOV3 cells. **C.** Cell migration and invasion were measured by transwell assays. **D.** Colony formation assays. **E.** Cell cycle percentage assays. **F.** Detection of apoptotic percentages. **G.** Detection of relevant protein expression by western blotting. **H.** Detection of the effect of LINC00665 and CNBP on the activity of the Wnt pathway. The relative fluorescence activity of each group of cells was assayed after transfection with TOPFlash/FOPFlash vectors: **a**. OCSCs with suppressed expression of LINC00665 and CNBP; **b**. COC1 and SKOV3 cells overexpressing LINC00665 and CNBP, $^{*}P < 0.05$

LINC00665 and CNBP (with all observed differences being statistically significant; Fig. 5B).

Patterns in the invasive, metastatic, and clonogenic potential of these cells were consistently observed. When LINC00665 was downregulated in OCSCs, there was a marked decrease in their ability to invade, metastasize, and form colonies compared to the control group. However, when both LINC00665 and CNBP expressions were inhibited, these cells demonstrated a significant increase in these capabilities compared to OCSCs with only LINC00665 downregulation. Furthermore, the forced expression of LINC00665 in COC1 and SKOV3 cells led to a notable enhancement in their invasive, metastatic, and colony-forming activities relative to the control. Yet, when LINC00665 and CNBP were both overexpressed in COC1 and SKOV3 cells, there was a reduction in these activities (Fig. 5C, D).

The suppression of LINC00665 alone in OCSCs resulted in a lower proportion of cells progressing to the S-phase and a higher rate of apoptosis when compared to the control. In contrast, OCSCs with both LINC00665 and CNBP suppression showed an increased entry into the S-phase and a reduced apoptotic rate compared to OCSCs with only LINC00665 downregulated. Conversely, the overexpression of LINC00665 alone significantly raised the percentage of COC1 cells entering the S-phase and lowered apoptosis rates. However, with the concurrent overexpression of LINC00665 and CNBP, there was a decline in the S-phase entry and an elevation in apoptosis among COC1 cells (Fig. 5E, F). These findings highlight the antagonistic roles of LINC00665 and CNBP in the modulation of stemness transition within ovarian cancer cells. LINC00665 appears to drive cell proliferation and reduce apoptosis by facilitating S-phase entry, and it also enhances invasion, metastasis, and colony formation, which can be counteracted by CNBP.

Subsequent investigations were directed at understanding the impact of CNBP and LINC00665 on the expression of stem cell markers, markers of epithelial-mesenchymal transition, and proteins involved in the Wnt signaling pathway, as well as their interplay in ovarian cancer cells. In OCSCs, the suppression of LINC00665 led to a cascade of molecular alterations: a reduction in the levels of stem cell markers (such as OCT4, SOX2, NANOG, ALDH1, and LGR5), as well as the cell surface markers (CD117 and CD133). Additionally, there was a decline in Ki-67 expression, indicative of a diminished proliferative ability of the cells. Concurrently, there was a downregulation of VE-cadherin, N-cadherin, and Vimentin, along with an upregulation of E-cadherin expression, pointing to a reduced potential for cell invasion and metastasis. The expression of MDR1, linked to multidrug resistance, and NOTCH1 also saw a decrease. The levels of nuclear β-catenin were lowered, while cytoplasmic β-catenin levels did not show significant alteration (Fig. 5G).

Concomitant inhibition of both LINC00665 and CNBP expression resulted in elevated levels of OCT4, SOX2, NANOG, ALDH1, LGR5, CD117, CD133, Ki-67, VE-cadherin, N-cadherin, Vimentin, NOTCH1, MDR1, and nuclear β-catenin proteins compared to cells with only LINC00665 suppression. Nevertheless, these expression levels were still below those observed in the control OCSCs. E-cadherin expression was found to be induced in the OCSCs group with only LINC00665 suppression but lower than in the OCSCs group with LINC00665 and CNBP inhibition. No significant changes were noted in the cytoplasmic β-catenin levels (Fig. 5G, left panel).

Elevating LINC00665 levels in COC1 and SKOV3 cells led to an increase in the expression of stem cell markers OCT4, SOX2, NANOG, ALDH1, LGR5, CD117, and CD133, as well as Ki-67, VE-cadherin, N-cadherin, Vimentin, NOTCH1, MDR1, and nuclear β-catenin. Conversely, E-cadherin expression was reduced, and cytoplasmic β-catenin levels remained unchanged (Fig. 5G). The augmentation of CNBP expression mitigated the upregulation effects of LINC00665 on these markers, with the exception of E-cadherin expression, which was marginally lower than the control group, and cytoplasmic β-catenin levels, which remained stable (Fig. 5G).

The transfection of TOPFlash/FOPFlash vectors into each cell group, followed by a dual-luciferase assay, indicated a reduction in fluorescence activity in OCSCs with LINC00665 knockdown, which was restored upon CNBP knockdown (Fig. 5H). In COC1 and SKOV3 cells with LINC00665 overexpression, fluorescence activity was increased, but this was attenuated when both LINC00665 and CNBP were overexpressed (Fig. 5H), suggesting that LINC00665 and CNBP exert reciprocal regulatory influences on the Notch and Wnt signaling pathways. In summary, we established that CNBP and LINC00665 assume antagonistic functions in the governance of stemness dynamics in ovarian cancer cells, with LINC00665 acting as a facilitator and CNBP serving as a repressor of this critical cellular transition. These results corroborate that LINC00665 participates in the regulation of the stemness of ovarian cancer cells by degrading *CNBP* mRNA through SMD.

In vivo modulation of CNBP and LINC00665 expression yields divergent effects on tumor development

In our investigation of the impact of CNBP and LINC00665 on tumorigenesis in vivo, we utilized a xenograft model with ovarian cancer stem cells in nude mice. The findings indicated that mice injected with OCSCs exhibiting increased CNBP and reduced LINC00665 (CNBP+/LINC00665-OCSC) developed smaller tumors compared to the control group. Notably, the group

receiving CNBP overexpression presented with the least tumor volume across all tested groups. In contrast, mice with dual suppression of both LINC00665 and CNBP (LINC00665-/CNBP-) exhibited a significant increase in tumor size relative to the group with only LINC00665 suppression (Fig. 6A, B, C).

Tumor tissue analysis showed an upsurge in CNBP mRNA and protein levels in mice injected with OCSC with suppressed LINC00665 expression (Supplementary Fig. 9). In these tumor samples, there was a notable decline in the levels of stem cell markers (OCT4, SOX2, NANOG, ALDH1, and LGR5), as well as cell surface markers (CD117 and CD133). This was accompanied by a reduction in Ki-67 expression, indicative of a decrease in cellular proliferation. Additionally, a decrease in VE-cadherin and an increase in E-cadherin expression were observed, suggesting a potential reduction in the invasive and metastatic capabilities of the cells. The expression of proteins associated with multidrug resistance, such as MDR1, CyclinD1, NOTCH1, and nuclear β-catenin, was also diminished, while cytoplasmic β-catenin levels remained unchanged. In neoplasms from the group with

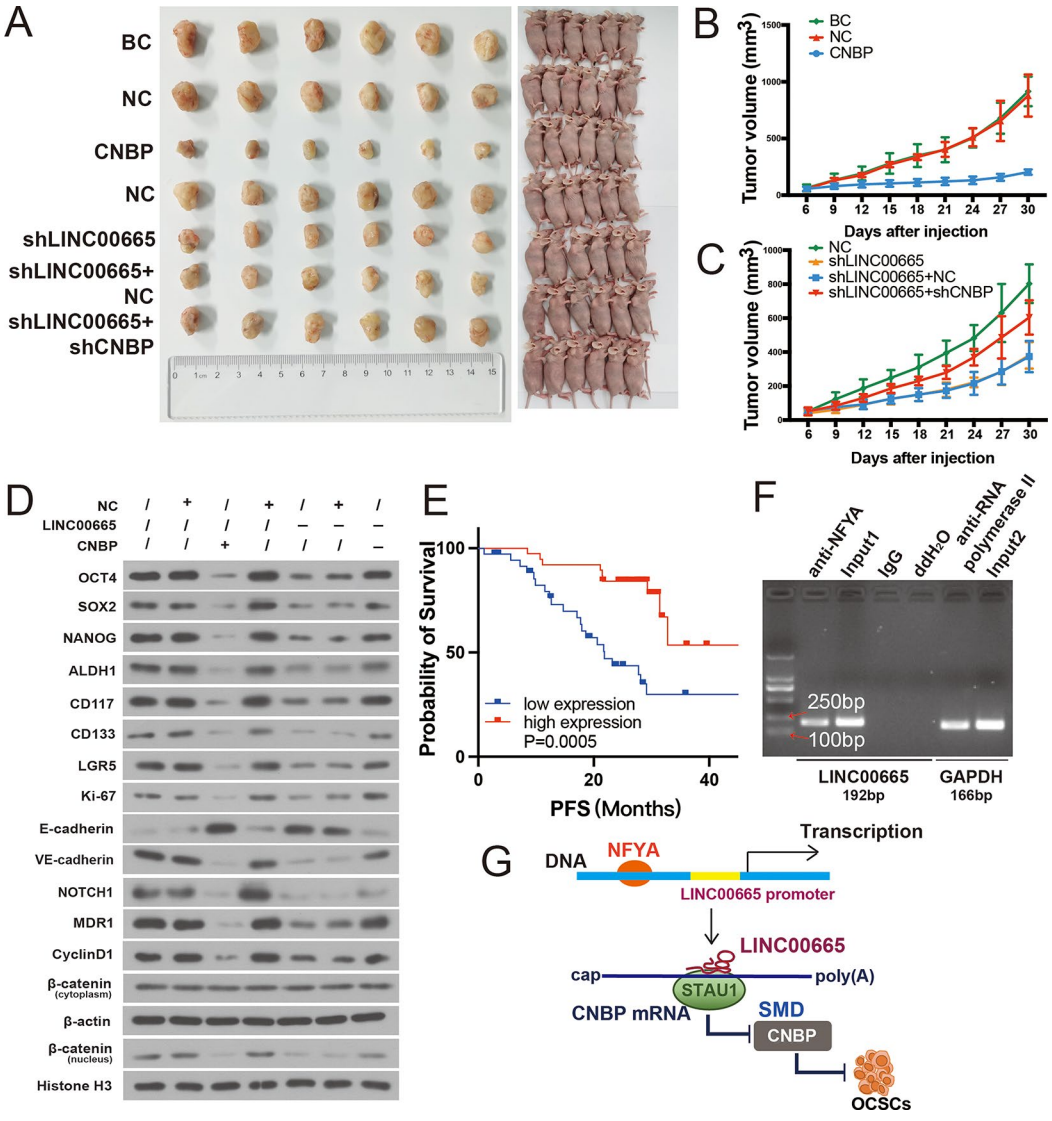

Fig. 6 Effect of CNBP and LINC00665 on ovarian cancer tumor growth in vivo**A.** Tumor-bearing nude mice and tumor samples from each group. **B.** Tumor volume was calculated every three days after injection. All tumors were excised four weeks after injection, and the tumor growth curve of CNBP-overexpressing OCSCs was compared with that of the control group. **C.** Comparison of tumor growth curves of OCSCs with LINC00665 inhibition alone or OCSCs with co-suppression of LINC00665 and CNBP expression with that of the control group. **D.** Expression of stemness marker proteins, proteins related to cell biological behaviors, and pathway proteins detected by western blotting. E. Disease-free survival analysis of ovarian cancer samples. The survival time of patients after surgery was compared between high-CNBP and low-CNBP expression groups. **F.** ChIP assay showing endogenous NFYA bound to the LINC00665 promoter in COC1 cells. **G**. LINC00665 increases CNBP degradation in OCSC via the SMD pathway to participate in OCSC stemness regulation, $^{*}P < 0.05$

diminished LINC00665 levels, there was a notable reduction in the expression of stem cell markers (OCT4, SOX2, NANOG, ALDH1, and LGR5), as well as cell surface markers (CD117 and CD133), coupled with a decrease in Ki-67 levels, indicating a suppression of cellular proliferation. Additional alterations in the tumor tissues included a decline in VE-cadherin levels, an increase in E-cadherin levels, and a reduction in MDR1, Cyclin D1, NOTCH1, and nuclear β-catenin levels. However, the levels of cytoplasmic β-catenin remained largely unchanged (Fig. 6D).

When comparing tumor samples from OCSC with only LINC00665 suppression to those from OCSCs with concurrent suppression of both LINC00665 and CNBP, the latter demonstrated elevated levels of OCT4, SOX2, NANOG, ALDH1, LGR5, CD117, CD133, Ki-67, VE-cadherin, NOTCH1, MDR1, CyclinD1, and nuclear β-catenin, along with a reduction in E-cadherin levels. The expression of cytoplasmic β-catenin, however, did not show significant variation (Fig. 6D). In line with these findings, an analysis of clinical data on ovarian cancer revealed that patients with higher CNBP expression exhibited longer periods of disease-free survival compared to those with lower CNBP expression ($P<0.05$, Fig. 6E). To further investigate the regulatory role of LINC00665 in ovarian cancer, the NCBI database was utilized to identify the sequence upstream of LINC00665's transcription start site, and the transcription factor 'NFYA' was predicted to bind to LINC00665 using the Jaspar online system. Primers were designed based on binding sites with high scores, and genomic DNA served as the template for PCR to confirm primer efficacy. A ChIP assay was conducted to validate the binding of NFYA to this site in COC1 cells (Fig. 6F). The comprehensive regulatory mechanism uncovered in this study is depicted in Fig. 6G.

Discussion

The ineffectiveness of ovarian cancer therapies is frequently linked to the emergence of chemoresistance, which encompasses both inherent resistance and acquired resistance, the latter being defined by relapse within six months following an initially successful treatment [36]. This phenomenon is notably prevalent among individuals receiving chemotherapy for ovarian cancer. A deeper investigation into the preservation of stemness features in OCSCs is imperative to elucidate the mechanisms behind the development and potential reversal of chemoresistance in ovarian cancer. In this study, we found that CNBP plays a suppressive role in the transition of stemness within ovarian cancer cells, while its expression is modulated by the SMD pathway driven by LINC00665. In the presence of STAU1, the 3'-UTR of *CNBP* mRNA and LINC00665 interact through matching Alu elements, forming a complex that leads to the SMD-mediated degradation of *CNBP* mRNA. This process influences the transition of stemness by impacting the Wnt and Notch signaling pathways (Fig. 6G).

The SMD pathway necessitates the presence of Alu elements within the lncRNA and the 3'-UTR of the corresponding mRNA [37]. Alu elements are unique sequences of nucleic acids that are widespread throughout the human genome, typically extending over roughly 300 base pairs [37]. These elements are predominantly located within intronic regions, the 3'-UTR, and intergenic spaces. Named for their inclusion of a specific recognition site (AGCT) at the 170 bp mark, which can be cleaved by the Alu I restriction enzyme, Alu elements can modulate the expression of protein-coding genes via cis-activation mechanisms during both transcription and translation [37]. The current research has uncovered a novel mechanism in ovarian cancer where the lncRNA LINC00665 exploits the SMD pathway to interact with and degrade *CNBP* mRNA. This discovery adds a new layer of understanding to the complex regulatory mechanisms that govern gene expression in ovarian cancer and may provide a basis for developing targeted therapies that disrupt this pathway.

LINC00665 has been identified as a key factor in a variety of tumors, with its abnormal expression being closely associated with clinical features and poor prognosis in several cancer types [38]. It can also significantly influence the response to chemotherapeutic agents such as gemcitabine, cisplatin, and paclitaxel [38]. Functioning as a competitive endogenous RNA (ceRNA), LINC00665 regulates cellular functions in cancer by acting as a molecular sponge for tumor-suppressive miRNAs, thus upregulating various oncogenes implicated in cancer progression. LINC00665 also influences the modulation of several key signaling cascades, such as Wnt/β-catenin, TGF-β, MAPK1, NF-κB, ERK, and PI3K/AKT, and it can enhance tumor metastasis by facilitating the epithelial-mesenchymal transition (EMT) process [39]. For instance, in ovarian cancer, LINC00665 upregulates the expression of genes like KLF5, E2F3, and FHDC by competitively binding with miRNA-148b-3p [40], miRNA-34a-5p [41], and miRNA-181a-5p [42], respectively, contributing to the progression of the disease. On the other hand, LINC00665 can inhibit the progression of triple-negative breast cancer [43] or encourage the progression of hepatocellular carcinoma by producing micropeptides [44]. Our study provides novel insights into the role of LINC00665 in ovarian cancer by identifying it as a crucial regulator of the multiple signaling pathways, which are related to cancer stemness. Unlike previous studies that primarily focused on in vitro experiments and specific miRNA axes, our research includes evidence demonstrating that LINC00665 can form duplex structures with the 3'-UTRs of target mRNAs

through the base pairing of Alu elements, regulating ovarian cancer development via STAU1-mediated mechanisms. This dual regulatory role, coupled with the modulation of multiple downstream molecular signaling pathways, highlights the complex molecular mechanisms by which LINC00665 promotes ovarian cancer progression. The inclusion of in vivo experiments provides a more comprehensive understanding of LINC00665's function, further proposing a promising and comprehensive approach to target LINC00665 for innovative therapeutic strategies in ovarian cancer.

Moreover, lncRNAs not only functions as a ceRNA, but they also can form duplex structures with the 3'-UTRs of target mRNAs through base pairing of Alu elements, playing a crucial role in the regulation of cancer development, progression, and spread via STAU1-mediated mechanisms [43–46] For instance, LINC00665 can form a physical complex with double-stranded RNA-activated protein kinase (PKR), enhancing its activation and preventing its degradation via the ubiquitin/proteasome pathway. This interaction stabilizes PKR, which in turn positively influences the NF-κB signaling cascade in hepatocellular carcinoma cells, ultimately fostering cancer development [49]. Additionally, evidence from glioma studies indicates that LINC00665 plays a role in controlling the malignant behaviors of glioma cells through the SMD pathway [50], further demonstrating LINC00665's ability to bind mRNA. In our research, we observed that LINC00665 levels were elevated in OCSCs compared to regular ovarian cancer cells. Utilizing RepeatMasker software, we pinpointed an Alu element within LINC00665. In situ hybridization experiments confirmed LINC00665's localization in the cytoplasm of ovarian cancer cells. Through the integration of GEO database and microarray analysis, we identified 1147 differentially expressed genes (DEGs) between OCSCs and ovarian cancer cells. Additionally, StarBase analysis helped us recognize 9 genes (*HKR1*, *SUN1*, *TMTC4*, *IDH1*, *CNBP*, *RBM19*, *EIF4A2*, *EEF1A1*, and *PSMD9*) with potential binding affinity to LINC00665. Notably, another RepeatMasker search uncovered an Alu element on the 3'-UTR of *CNBP* mRNA, which could engage in partial base pairing with the Alu element on LINC00665. Using MS2-RIP and RIP assays in the presence of STAU1, we confirmed the interaction between the Alu element of LINC00665 and the Alu element on the 3'-UTR of *CNBP* mRNA. We further established that LINC00665 facilitates the degradation of CNBP mRNA via this interaction, thereby exerting post-transcriptional control over CNBP expression. Thus, out study adds to this body of knowledge by demonstrating that LINC00665 promotes the degradation of *CNBP* mRNA in ovarian cancer stem cells, thereby regulating cancer stemness and contributing to the malignancy of ovarian cancer.

CNBP, a highly conserved nucleic acid-binding protein, possesses seven zinc finger motifs of the CCHC type and a region abundant in arginine and glycine (RG/RGG) [19, 51]. This protein is capable of binding to single-stranded nucleic acids, playing a role in the regulation of disorders such as neuromuscular degeneration, inflammation, autoimmune conditions, and various cancers [19, 51]. Significantly, CNBP has an affinity for guanine (G)-rich sequences in DNA and RNA that can form G-quadruplexes (G4), secondary structures that serve as regulatory elements influencing gene transcription near transcription start sites or modulating translation on mRNAs [19, 51]. Proteins that can modulate G4 structures are thus promising targets for cancer therapy. CNBP specifically binds to sequences containing GGAG [52], functioning as a nucleic acid chaperone that rearranges secondary structures, impacting biological processes by altering chromatin or RNA configurations. Within the cell nucleus, CNBP plays a role in transcriptional regulation, unwinding G4 structures at gene promoters to control the expression of downstream genes [53]. For instance, CNBP is known to upregulate the transcription of KRAS and c-MYC, while downregulating NOG/nog3 by resolving G4 structures at their respective promoter regions, influencing the process of tumorigenesis [54]. CNBP can also induce the formation of G4 structures, as seen when its overexpression leads to the suppression of hnRNP K transcription through G4 structure induction at its promoter, reducing the malignancy and invasiveness of fibrosarcoma cells [55]. In the context of hepatocellular carcinoma, CNBP's interaction with the *PGM1* promoter encourages G4 structure formation, which decreases PGM1 expression, affects glucose metabolism, and thus hampers cancer progression [56]. Cytoplasmically, CNBP is involved in RNA stability regulation, capable of dismantling stable G4 structures in mRNAs to enhance translation without altering mRNA levels [52]. It also aids in the resolution of G4 structures in viral RNA, such as the SARS-CoV-2 genome, facilitating the synthesis of viral proteins [57]. Recent discoveries have unveiled novel mechanisms by which CNBP modulates RNA stability. Research in pancreatic ductal adenocarcinoma revealed that CNBP can recognize m6A-modified RNA and enhance its stability [58]. By binding to the 5'-UTR of mRNA, CNBP collaborates with a lncRNA to enhance mRNA stability, thereby promoting cell division and proliferation in tumor cells [59]. This multifaceted role of CNBP in gene regulation, both at the level of transcription and mRNA stability, underscores its potential as a therapeutic target in various diseases, including cancer.

Despite the lack of extensive research on the role and regulatory mechanisms of CNBP in ovarian cancer, particularly its involvement in the regulation of stemness transition, this study has revealed that elevated CNBP

levels have diagnostic significance in epithelial ovarian cancer. The expression of CNBP may serve as an indicator of the response to chemotherapy, offering potential clinical utility not only in treatment but also in diagnosis and predicting the effectiveness of chemotherapy. The resistance of tumors to chemotherapeutic agents, such as drug resistance, is associated with the stem cell-like characteristics of tumor cells. Consequently, our research shifted focus to the interplay between CNBP and the stem cell attributes of ovarian cancer cells. Our findings indicate that CNBP acts as a negative regulator of the stemness transition in ovarian cancer cells, and higher CNBP expression diminishes the expression of stem cell markers and disrupts the maintenance of stemness in these cells. Additionally, elevated CNBP levels were found to inhibit key genes and their activity within the Wnt, Notch, and other pathways, suggesting that its inhibitory effect on stemness transition may be mediated through these pathways. We also observed that CNBP could influence the concentration of β-catenin within the nucleus without notably altering its cytoplasmic levels. Thus, we hypothesize that CNBP may either prevent the nuclear import of β-catenin or enhance its degradation within the nucleus, consequently inhibiting the interaction of β-catenin with TCF/LEF and the subsequent transcription of Wnt pathway target genes. This hypothesis warrants further investigation for validation.

Recent research has shed light on a spectrum of post-transcriptional regulatory mechanisms that influence CNBP's function in various cancers. For instance, the ceRNA mechanism is instrumental in the post-transcriptional control of CNBP expression, as seen in colorectal cancer cells where CircPACRGL captures miRNA-330-3p, thereby modulating tumor proliferation through the miRNA-330-3p/CNBP pathway [60]. Methylation also plays a critical role, with PRMT1 in HeLa cells methylating CNBP's arginine- and glycine-rich segment, a modification that, despite not altering CNBP's nuclear localization, restricts its ability to bind RNA and consequently reduces its activity [61]. In the realm of drug resistance, CircFMN2 contributes to heightened sorafenib resistance in multidrug-resistant hepatocellular carcinoma by blocking CNBP ubiquitination, leading to increased CNBP expression [62]. Phosphorylation is another regulatory factor, and phosphorylated CNBP enhances the annealing of oligonucleotides to the CT element of the c-MYC promoter, thereby acting as a transcriptional enhancer for c-MYC [63]. Furthermore, the phosphorylation of CNBP by AMP-activated protein kinase, triggered by Hedgehog pathway activation in adult neural tube cell tumors, strengthens the CNBP-Sufu interaction, stabilizes CNBP, and decreases its proteasomal degradation, which is linked to the proliferation of medulloblastoma cells. Lastly, redox proteomics have detected increased CNBP oxidation in various tumors [64], suggesting that CNBP-Cys oxidation is a crucial aspect of redox homeostasis in tumorigenesis [51]. Although it has been demonstrated that the pre-mRNA of CNBP is regulated by alternative splicing and has multiple isoforms, no structural or functional differences between these isoforms have been reported [51]. Our study identified a novel mechanism in which LINC00665 and STAU1 degrade *CNBP* mRNA through the SMD pathway and thereby regulate CNBP expression. This mechanism can release the inhibition of Wnt, Notch, and other pathways resulting from the increased CNBP expression, promoting ovarian cancer cell stemness transition.

Our findings indicated that CNBP expression is elevated in malignant tumors relative to benign ones, yet it is reduced in OCSCs compared to non-stem ovarian cancer cells, suggesting a link to tumor heterogeneity. This heterogeneity could be shaped by the cellular microenvironment, genetic and epigenetic factors, with CSCs contributing to the diversity within tumor cell subpopulations and initiating tumorigenesis [65]. In colorectal cancer (CRC), E-cadherin exhibits strong positivity across primary lesions, metastatic peritoneal tissues, and malignant ascites cells. However, Tamura, S. et al. identified CRC pathological subtypes with varying E-cadherin levels, where E-cadherin positive (EC+) CSCs displayed a higher in vivo proliferation potential than E-cadherin negative (EC-) CSCs, potentially due to elevated NANOG-driven cyclin D1 and B1 expression. Conversely, EC- CSCs, characterized by low cyclin D1 expression, are considered quiescent and capable of reverting to EC+status depending on their microenvironment [66]. Genetic reprogramming during tumor progression may influence SCs/CSCs behavior, preserving SC pluripotency and driving differentiation [67, 68]. KRT19's role in cancer progression is paradoxical; it is upregulated in both colon and breast cancers, yet its suppression leads to divergent outcomes. In colon cancer, KRT19 downregulation hampers tumor growth by attenuating Wnt/Notch signaling without affecting NUMB transcription. In contrast, breast cancer experiences increased malignancy characteristics upon KRT19 knockdown due to diminished Wnt signaling and augmented Notch signaling [69]. Further research has linked high KRT19 expression in breast cancer to invasiveness, while breast cancer-derived CSCs with high CD133/CXCR4/ALDH1 expression show low KRT19 and high NOTCH1 levels, implicating KRT19 in CSC reprogramming and drug sensitivity regulation [70, 71]. Moreover, KRT19's impact varies between HER2+and HER2- breast cancer subtypes [72, 73]. Collectively, these findings underscore that not all cells within a line express uniform stemness levels but rather exhibit a plasticity

influenced by their microenvironment [74]. Our data suggest CNBP's role in inhibiting OCSC stemness, yet its regulatory function may differ from that of OCSCs compared to other ovarian cancer cells at different stages of tumorigenesis and development or within different microenvironments. While CNBP expression in ovarian cancer tissues was found to be higher than in serous cystadenoma in our study, analysis of TCGA and GTEx data suggested that CNBP expression in epithelial ovarian cancer is lower than in normal ovarian tissues. This discrepancy indicates that CNBP may have distinct roles in normal ovarian tissue, ovarian serous cystadenoma, and ovarian cancer, necessitating further investigation.

Conclusion

Our investigation has uncovered a previously unrecognized pathway in ovarian cancer, wherein LINC00665 engages *CNBP* mRNA via a STAU1-dependent mechanism, culminating in mRNA degradation. This axis is crucial for the control of stemness in ovarian cancer cells, with CNBP playing a significant role in this process. These findings pave the way for novel therapeutic strategies, proposing that disrupting the LINC00665-STAU1 interaction with targeted inhibitors, including small molecules, might provide an effective means to combat drug resistance and avert ovarian cancer relapse by altering the stem-like qualities of the cancer cells.

Abbreviations

CSCs	Cancer stem cells
CNBP	CCHC-type zinc finger nucleic acid binding protein
DEGs	Differentially expressed genes
DELs	Differentially expressed lncRNAs
lncRNA	Long non-coding RNA
OCSCs	Ovarian cancer stem cells
OS	Overall survival
PKR	RNA-activated protein kinase
SMD	Staufen-mediated mRNA decay

Supplementary Information

The online version contains supplementary material available at https://doi.org/10.1186/s13062-024-00506-w.

Supplementary Material 1

Supplementary Material 2

Supplementary Material 3

Supplementary Material 4

Acknowledgements

Not applicable.

Author contributions

Conceptualization, methodology, funding acquisition were performed by YZ and YD; sample collection was performed by MW; experiment was performed by XL, YC and YL; data analyze was performed by XL, JB and ZZ; writing-original draft was performed by XL, YC and YL; figures and/or tables prepare was performed by MW and JB; writing-reviewing and editing was performed by YZ. All authors read and approved the final manuscript.

Funding

This study was supported by grants from the National Natural Science Foundation of China for Young Scientists of China (Grant No. 81902658, YZ; Grant No. 82303040, XL); the National Natural Science Foundation of China (Grant No. 92168115); the Science Foundation for Outstanding Young Scholars of Liaoning Province (Grant No. 2022-YQ-16, YD); 345 Talent Project of Shengjing Hospital (Grant No. M1400, YD); and the Project of City-University Cooperation (Grant No. 2400022047, YD); Liaoning Province Science and Technology Plan Joint Program Project (Grant No. 2023JH2/101700105, XL).

Data availability

The datasets generated during and/or analyzed during the current study are available in the UCSC database repository, (TCGA TARGET GTEx (PANCAN, *N*=19131, G=60499), https://xenabrowser.net/).

Declarations

Ethics approval and consent to participate

This study was performed in line with the principles of the Declaration of Helsinki. Approval was granted by the Ethics Committee of China Medical University [No. 2019PS286K(X1) and No. 2019PS285K(X1)]. Informed consent was obtained from all individual participants included in the study.

Consent for publication

The authors affirm that human research participants provided informed consent for publication of the images in Fig. 1B.

Competing interests

The authors declare no competing interests.

Received: 1 February 2024 / Accepted: 22 July 2024
Published online: 30 July 2024

References

1. Li C, Heidt DG, Dalerba P, Burant CF, Zhang L, Adsay V, Wicha M, Clarke MF, Simeone DM. Identification of pancreatic cancer stem cells. Cancer Res. 2007;67(3):1030–7.
2. Valent P, Bonnet D, De Maria R, Lapidot T, Copland M, Melo JV, Chomienne C, Ishikawa F, Schuringa JJ, Stassi G, et al. Cancer stem cell definitions and terminology: the devil is in the details. Nat Rev Cancer. 2012;12(11):767–75.
3. Ahmed N, Abubaker K, Findlay J, Quinn M. Cancerous ovarian stem cells: obscure targets for therapy but relevant to chemoresistance. J Cell Biochem. 2013;114(1):21–34.
4. Balic M, Lin H, Young L, Hawes D, Giuliano A, McNamara G, Datar RH, Cote RJ. Most early disseminated cancer cells detected in bone marrow of breast cancer patients have a putative breast cancer stem cell phenotype. Clin Cancer Res. 2006;12(19):5615–21.
5. Bao S, Wu Q, Sathornsumetee S, Hao Y, Li Z, Hjelmeland AB, Shi Q, McLendon RE, Bigner DD, Rich JN. Stem cell-like glioma cells promote tumor angiogenesis through vascular endothelial growth factor. Cancer Res. 2006;66(16):7843–8.
6. Louie E, Nik S, Chen JS, Schmidt M, Song B, Pacson C, Chen XF, Park S, Ju J, Chen EI. Identification of a stem-like cell population by exposing metastatic breast cancer cell lines to repetitive cycles of hypoxia and reoxygenation. Breast Cancer Res. 2010;12(6):R94.
7. Todaro M, Alea MP, Di Stefano AB, Cammareri P, Vermeulen L, Iovino F, Tripodo C, Russo A, Gulotta G, Medema JP, et al. Colon cancer stem cells dictate tumor growth and resist cell death by production of interleukin-4. Cell Stem Cell. 2007;1(4):389–402.
8. Lee HH, Bellat V, Law B. Chemotherapy induces adaptive drug resistance and metastatic potentials via phenotypic CXCR4-expressing cell state transition in ovarian cancer. PLoS ONE. 2017;12(2):e0171044.
9. Cheung TH, Rando TA. Molecular regulation of stem cell quiescence. Nat Rev Mol Cell Biol. 2013;14(6):329–40.
10. Sun Z, Wang L, Dong L, Wang X. Emerging role of exosome signalling in maintaining cancer stem cell dynamic equilibrium. J Cell Mol Med. 2018;22(8):3719–28.

11. Funakoshi K, Bagheri M, Zhou M, Suzuki R, Abe H, Akashi H. Highly sensitive and specific Alu-based quantification of human cells among rodent cells. Sci Rep. 2017;7(1):13202. https://doi.org/10.1038/s41598-017-13402-3.
12. Batzer MA, Deininger PL. Alu repeats and human genomic diversity. Nat Rev Genet. 2002;3(5):370–9. https://doi.org/10.1038/nrg798.
13. Yao RW, Wang Y, Chen LL. Cellular functions of long noncoding RNAs. Nat Cell Biol. 2019;21(5):542–51. https://doi.org/10.1038/s41556-019-0311-8.
14. Gong C, Maquat LE. lncRNAs Transactivate STAU1-mediated mRNA decay by duplexing with 3' UTRs via Alu elements. Nature. 2011;470(7333):284–8.
15. Kim YK, Furic L, Parisien M, Major F, DesGroseillers L, Maquat LE. Staufen1 regulates diverse classes of mammalian transcripts. Embo j. 2007;26(11):2670–81.
16. Kim YK, Furic L, Desgroseillers L, Maquat LE, Mammalian Staufen1 recruits Upf1 to specific mRNA 3'UTRs so as to elicit mRNA decay. Cell
17. Kim YK, Furic L, Desgroseillers L, Maquat LE, Mammalian Staufen1 recruits Upf1 to specific mRNA 3'UTRs so as to elicit mRNA decay. Cell
18. Damas ND, Marcatti M, Côme C, Christensen LL, Nielsen MM, Baumgartner R, Gylling HM, Maglieri G, Rundsten CF, Seemann SE, et al. SNHG5 promotes colorectal cancer cell survival by counteracting STAU1-mediated mRNA destabilization. Nat Commun 2016;7(13875).
19. Armas P, Coux G, Weiner AMJ, Calcaterra NB. What's new about CNBP? Divergent functions and activities for a conserved nucleic acid binding protein. Biochim Biophys Acta Gen Subj. 2021;1865(11):129996. https://doi.org/10.1016/j.bbagen.2021.129996.
20. Lee E, Lee TA, Yoo HJ, Lee S, Park B. CNBP controls tumor cell biology by regulating tumor-promoting gene expression. Mol Carcinog. 2019;58(8):1492–501. https://doi.org/10.1002/mc.23030.
21. Gao L, Li X, Nie X, Guo Q, Liu Q, Qi Y, Liu J, Lin B. Construction of novel mRNA-miRNA-lncRNA regulatory networks associated with prognosis of ovarian cancer. J Cancer. 2020;11(23):7057–72. https://doi.org/10.7150/jca.49557.
22. Ma L, Lai D, Liu T, Cheng W, Guo L. Cancer stem-like cells can be isolated with drug selection in human ovarian cancer cell line SKOV3. Acta Biochim Biophys Sin (Shanghai). 2010;42(9):593–602.
23. Teramura T, Fukuda K, Kurashimo S, Hosoi Y, Miki Y, Asada S, Hamanishi C. Isolation and characterization of side population stem cells in articular synovial tissue. BMC Musculoskelet Disord. 2008;9:86.
24. Lánczky A, Győrffy B. Web-based Survival Analysis Tool tailored for Medical Research (KMplot): development and implementation. J Med Internet Res. 2021;23(7):e27633.
25. Szotek PP, Pieretti-Vanmarcke R, Masiakos PT, Dinulescu DM, Connolly D, Foster R, Dombkowski D, Preffer F, Maclaughlin DT, Donahoe PK. Ovarian cancer side population defines cells with stem cell-like characteristics and mullerian inhibiting substance responsiveness. Proc Natl Acad Sci U S A. 2006;103(30):11154–9.
26. Alvero AB, Chen R, Fu HH, Montagna M, Schwartz PE, Rutherford T, Silasi DA, Steffensen KD, Waldstrom M, Visintin I, et al. Molecular phenotyping of human ovarian cancer stem cells unravels the mechanisms for repair and chemoresistance. Cell Cycle. 2009;8(1):158–66.
27. Lee YJ, Wu CC, Li JW, Ou CC, Hsu SC, Tseng HH, Kao MC, Liu JY. A rational approach for cancer stem-like cell isolation and characterization using CD44 and prominin-1(CD133) as selection markers. Oncotarget. 2016;7(48):78499–515.
28. Zhang S, Balch C, Chan MW, Lai HC, Matei D, Schilder JM, Yan PS, Huang TH, Nephew KP. Identification and characterization of ovarian cancer-initiating cells from primary human tumors. Cancer Res. 2008;68(11):4311–20.
29. Cao J. The functional role of long non-coding RNAs and epigenetics. Biol Proced Online. 2014;16:11.
30. Perry RB, Ulitsky I. The functions of long noncoding RNAs in development and stem cells. Development. 2016;143(21):3882–94.
31. Eades G, Zhang YS, Li QL, Xia JX, Yao Y, Zhou Q. Long non-coding RNAs in stem cells and cancer. World J Clin Oncol. 2014;5(2):134–41.
32. Li W, Zhang L, Guo B, Deng J, Wu S, Li F, Wang Y, Lu J, Zhou Y. Exosomal FMR1-AS1 facilitates maintaining cancer stem-like cell dynamic equilibrium via TLR7/NFκB/c-Myc signaling in female esophageal carcinoma. Mol Cancer. 2019;18(1):22.
33. Lin Y, Pan X, Shen HB. lncLocator 2.0: a cell-line-specific subcellular localization predictor for long non-coding RNAs with interpretable deep learning. Bioinformatics. 2021;37(16):2308–16.
34. Li JH, Liu S, Zhou H, Qu LH, Yang JH. starBase v2.0: decoding miRNA-ceRNA, miRNA-ncRNA and protein-RNA interaction networks from large-scale CLIP-Seq data. Nucleic Acids Res. 2014;42(Database issue):D92–7.
35. Fekete JT, Győrffy B. ROCplot.org: validating predictive biomarkers of chemotherapy/hormonal therapy/anti-HER2 therapy using transcriptomic data of 3,104 breast cancer patients. Int J Cancer. 2019;145(11):3140–51.
36. Na YJ, Farley J, Zeh A, del Carmen M, Penson R, Birrer MJ. Ovarian cancer: markers of response. Int J Gynecol Cancer. 2009;19(Suppl 2):21–9.
37. Gussakovsky D, McKenna SA. Alu RNA and their roles in human disease states. RNA Biol. 2021;18(sup2):574–85. https://doi.org/10.1080/15476286.2021.1989201.
38. Zhong C, Xie Z, Shen J, Jia Y, Duan S. LINC00665: an emerging biomarker for Cancer Diagnostics and therapeutics. Cells 2022;11(9).
39. Ghafouri-Fard S, Khoshbakht T, Hussen BM, Baniahmad A, Taheri M, Hajiesmaeili M. A Concise Review on Dysregulation of LINC00665 in cancers. Cells 2022;11(22).
40. Wang S, Liu C, Li Y, Qiao J, Chen X, Bao J, Li R, Xing Y. LINC00665 affects the malignant biological behavior of ovarian cancer via the miR-148b-3p/KLF5. Syst Biol Reprod Med. 2022;68(5–6):370–83.
41. Xu D, Song Q, Liu Y, Chen W, Lu L, Xu M, Fang X, Zhao W, Zhou H. LINC00665 promotes ovarian Cancer progression through regulating the miRNA-34a-5p/E2F3 axis. J Cancer. 2021;12(6):1755–63.
42. Wang S, Wang Y, Lu J, Wang J. LncRNA LINC00665 promotes ovarian Cancer Cell Proliferation and inhibits apoptosis via Targeting miR-181a-5p/FHDC. Appl Biochem Biotechnol. 2022;194(9):3819–32.
43. Guo B, Wu S, Zhu X, Zhang L, Deng J, Li F, Wang Y, Zhang S, Wu R, Lu J, et al. Micropeptide CIP2A-BP encoded by LINC00665 inhibits triple-negative breast cancer progression. Embo j. 2020;39(1):e102190.
44. Li YR, Zong RQ, Zhang HY, Meng XY, Wu FX. Mechanism analysis of LINC00665 and its peptides CIP2A-BP in Hepatocellular Carcinoma. Front Genet. 2022;13:861096.
45. Chen C, Shen N, Chen Y, Jiang P, Sun W, Wang Q, Wang Z, Jiang Y, Cheng W, Fu S et al. LncCCLM inhibits lymphatic metastasis of cervical cancer by promoting STAU1-mediated IGF-1 mRNA degradation. Cancer Lett 2021;518(169 – 79.
46. Su R, Ma J, Zheng J, Liu X, Liu Y, Ruan X, Shen S, Yang C, Wang D, Cai H, et al. PABPC1-induced stabilization of BDNF-AS inhibits malignant progression of glioblastoma cells through STAU1-mediated decay. Cell Death Dis. 2020;11(2):81.
47. Jing F, Ruan X, Liu X, Yang C, Wang D, Zheng J, Xue Y, Shen S, Shao L, Yang Y et al. The PABPC5/HCG15/ZNF331 feedback Loop regulates Vasculogenic Mimicry of Glioma via STAU1-Mediated mRNA decay. Mol Ther Oncolytics 2020;17(216 – 31.
48. Zhao L, Jiang L, Zhang M, Zhang Q, Guan Q, Li Y, He M, Zhang J, Wei M. NF-κB-activated SPRY4-IT1 promotes cancer cell metastasis by down-regulating TCEB1 mRNA via Staufen1-mediated mRNA decay. Oncogene. 2021;40(30):4919–29.
49. Ding J, Zhao J, Huan L, Liu Y, Qiao Y, Wang Z, Chen Z, Huang S, Zhao Y, He X. Inflammation-Induced Long Intergenic noncoding RNA (LINC00665) increases Malignancy through activating the double-stranded RNA-Activated protein Kinase/Nuclear factor Kappa B pathway in Hepatocellular Carcinoma. Hepatology. 2020;72(5):1666–81.
50. Ruan X, Zheng J, Liu X, Liu Y, Liu L, Ma J, He Q, Yang C, Wang D, Cai H et al. lncRNA LINC00665 stabilized by TAF15 impeded the malignant Biological behaviors of Glioma cells via STAU1-Mediated mRNA degradation. Mol Ther Nucleic Acids 2020;20(823 – 40.
51. Rajavashisth TB, Taylor AK, Andalibi A, Svenson KL, Lusis AJ. Identification of a zinc finger protein that binds to the sterol regulatory element. Science. 1989;245(4918):640–3. https://doi.org/10.1126/science.2562787.
52. Benhalevy D, Gupta SK, Danan CH, Ghosal S, Sun HW, Kazemier HG, Paeschke K, Hafner M, Juranek SA. The human CCHC-type zinc finger nucleic acid-binding protein binds G-Rich elements in target mRNA coding sequences and promotes translation. Cell Rep. 2017;18(12):2979–90.
53. Ghosal G, Muniyappa K. Hoogsteen base-pairing revisited: resolving a role in normal biological processes and human diseases. Biochem Biophys Res Commun. 2006;343(1):1–7.
54. David AP, Pipier A, Pascutti F, Binolfi A, Weiner AMJ, Challier E, Heckel S, Calsou P, Gomez D, Calcaterra NB, et al. CNBP controls transcription by unfolding DNA G-quadruplex structures. Nucleic Acids Res. 2019;47(15):7901–13.
55. Qiu J, Chen S, Su L, Liu J, Xiao N, Ou TM, Tan JH, Gu LQ, Huang ZS, Li D. Cellular nucleic acid binding protein suppresses tumor cell metastasis and induces tumor cell death by downregulating heterogeneous ribonucleoprotein K in fibrosarcoma cells. Biochim Biophys Acta. 2014;1840(7):2244–52.
56. Jin GZ, Zhang Y, Cong WM, Wu X, Wang X, Wu S, Wang S, Zhou W, Yuan S, Gao H, et al. Phosphoglucomutase 1 inhibits hepatocellular carcinoma progression by regulating glucose trafficking. PLoS Biol. 2018;16(10):e2006483.

57. Bezzi G, Piga EJ, Binolfi A, Armas P. CNBP binds and unfolds in Vitro G-Quadruplexes formed in the SARS-CoV-2 positive and negative genome strands. Int J Mol Sci 2021;22(5).
58. Deng J, Zhang J, Ye Y, Liu K, Zeng L, Huang J, Pan L, Li M, Bai R, Zhuang L, et al. N(6) -methyladenosine-mediated upregulation of WTAPP1 promotes WTAP translation and wnt signaling to facilitate pancreatic Cancer progression. Cancer Res. 2021;81(20):5268–83.
59. Cao L, Zhang P, Li J, Wu M. LAST, a c-Myc-inducible long noncoding RNA, cooperates with CNBP to promote CCND1 mRNA stability in human cells. Elife 2017;6(.
60. Liu H, Fang Y, Hou B, Lin Q, Zhang W, Wang X, Hu Y, Xu G, He Z. CircPACRGL promoted cell proliferation, migration and invasion as well as inhibited cell apoptosis in colorectal cancer via regulation of the miR-330-3p/CNBP axis. Mol Cell Biochem. 2023;478(7):1633–44.
61. Wei HM, Hu HH, Chang GY, Lee YJ, Li YC, Chang HH, Li C. Arginine methylation of the cellular nucleic acid binding protein does not affect its subcellular localization but impedes RNA binding. FEBS Lett. 2014;588(9):1542–8.
62. Fan C, Zhu X, Zhou Q, Wang W. CircFMN2 boosts Sorafenib Resistance in Hepatocellular Carcinoma cells via upregulating CNBP by restraining Ubiquitination. J Oncol. 2022;2022:2674163.
63. Lombardo VA, Armas P, Weiner AM, Calcaterra NB. In vitro embryonic developmental phosphorylation of the cellular nucleic acid binding protein by cAMP-dependent protein kinase, and its relevance for biochemical activities. Febs j. 2007;274(2):485–97.
64. D'Amico D, Antonucci L, Di Magno L, Coni S, Sdruscia G, Macone A, Miele E, Infante P, Di Marcotullio L, De Smaele E, et al. Non-canonical Hedgehog/AMPK-Mediated Control of Polyamine Metabolism supports neuronal and Medulloblastoma Cell Growth. Dev Cell. 2015;35(1):21–35.
65. Kim HK, Yang Y, Byeon S, Jeong Y, Kwon J, Lee KH, Son SM, Han HS. E-Cadherin and Angiopoietin-2 as potential biomarkers for Colorectal Cancer with Peritoneal Carcinomatosis. Anticancer Res. 2021;41(9):4497–504.
66. Tamura S, Isobe T, Ariyama H, Nakano M, Kikushige Y, Takaishi S, Kusaba H, Takenaka K, Ueki T, Nakamura M, et al. E–cadherin regulates proliferation of colorectal cancer stem cells through NANOG. Oncol Rep. 2018;40(2):693–703.
67. Chestkov IV, Khomyakova EA, Vasilieva EA, Lagarkova MA, Kiselev SL. Molecular barriers to processes of genetic reprogramming and cell transformation. Biochem (Mosc). 2014;79(12):1297–307.
68. Bogomazova AN, Vassina EM, Kiselev SI, Lagarkova MA, Lebedeva OS, Nekrasov ED, Panova AV, Philonenko ES, Khomyakova EA, Tskhovrebova LV, et al. [Genetic cell reprogramming: a New Technology for Basic Research and Applied usage]. Genetika. 2015;51(4):466–78.
69. Saha SK, Yin Y, Chae HS, Cho SG. Opposing regulation of Cancer properties via KRT19-Mediated Differential Modulation of Wnt/β-Catenin/Notch signaling in breast and Colon cancers. Cancers (Basel) 2019;11(1).
70. Saha SK, Choi HY, Kim BW, Dayem AA, Yang GM, Kim KS, Yin YF, Cho SG. KRT19 directly interacts with β-catenin/RAC1 complex to regulate NUMB-dependent NOTCH signaling pathway and breast cancer properties. Oncogene. 2017;36(3):332–49.
71. Saha SK, Kim K, Yang GM, Choi HY, Cho SG. Cytokeratin 19 (KRT19) has a role in the reprogramming of Cancer Stem Cell-Like cells to less aggressive and more drug-sensitive cells. Int J Mol Sci 2018;19(5).
72. Ju JH, Yang W, Lee KM, Oh S, Nam K, Shim S, Shin SY, Gye MC, Chu IS, Shin I. Regulation of cell proliferation and migration by keratin19-induced nuclear import of early growth response-1 in breast cancer cells. Clin Cancer Res. 2013;19(16):4335–46.
73. Ju JH, Oh S, Lee KM, Yang W, Nam KS, Moon HG, Noh DY, Kim CG, Park G, Park JB, et al. Cytokeratin19 induced by HER2/ERK binds and stabilizes HER2 on cell membranes. Cell Death Differ. 2015;22(4):665–76.
74. Ferrara B, Dugnani E, Sordi V, Pasquale V, Pellegrini S, Reni M, Balzano G, Piemonti L. A Comprehensive characterization of stemness in cell lines and primary cells of pancreatic ductal adenocarcinoma. Int J Mol Sci 2022;23(18).

Publisher's Note